P865: REVISED LETTER OF INTENT
for a
HIGH-SENSITIVITY STUDY OF CHARM AND BEAUTY DECAYS

L. D. Isenhower, M. E. Sadler
Abilene Christian University

D. Chrisman, D. Cline, J. Park, J. Rhoades
University of California at Los Angeles

L. Diaz-Cruz, M. Perez, J. Toscano
CINVESTAV-IPN, Mexico City

M. Atac
Fermilab and University of California at Los Angeles

C. N. Brown, W. E. Cooper
Fermilab

L. M. Lederman
Illinois Institute of Technology

H. B. Crawley, A. Firestone, J. W. Lamsa, W. T. Meyer, E. I. Rosenberg
Iowa State University

D. M. Kaplan
Northern Illinois University

R. C. Childers, C. W. Darden, J. R. Wilson
University of S. Carolina

R. C. Chaney, E. J. Fenyves, J. R. Friedrich, H. Hammack, J. Orgeron
University of Texas at Dallas

and the

Optical Trigger Collaboration:

G. Charpak
CERN

Y. Giomataris, C. Joseph, C. Morel, J.-P. Perroud, M. T. Tran
Université de Lausanne

R. Chipaux, J. Derré, C. Kochowski, Y. Lemoigne, S. Loucatos, Ph. Rebourgeard
CEN Saclay

Spokesperson:

Daniel M. Kaplan

April 2, 1993

ABSTRACT

We propose a comprehensive study of charm and beauty decays, to be carried out using a high-rate open-geometry spectrometer. The spectrometer will be assembled in stages over the next two fixed-target runs. It will differ from existing open-geometry spectrometers in several important respects, including: 1) the use of a small beam and target, with a small beam hole extending through the apparatus, to maximize the rate capability; 2) high-rate high-resolution tracking based on scintillating fibers; 3) efficient triggering based on decay-vertex topology and the presence of high-transverse-momentum secondaries; and 4) hadron identification by means of a unique high-rate ring-imaging Cherenkov counter. Our goal for the next two fixed-target runs is the study of $\sim 10^{14}$ interactions, yielding fully-reconstructed samples of $\sim 10^7 - 10^8$ charm and $\sim 10^4$ beauty decays. A novel optical impact-parameter 1st-level trigger facilitates operation at the 50 MHz interaction rate required for such sensitivity. The large acceptance and high tagging efficiency of the proposed spectrometer will provide unique samples of tagged events, permitting observation of B_s–$\bar{B}_s$ mixing and extraction of absolutely-normalized charm branching ratios. Additional issues to be addressed include rare beauty decays such as $B \to X\gamma$, $\ell^+\ell^- X$, $\pi\pi$, πK, $\pi\rho$, $K\rho$, etc. as well as rare charm decays, $D\bar{D}$ mixing, and CP violation in the charm sector. Our long-term goal is observation of CP violation in B decay, which we may achieve by the end of the decade if we can develop techniques for increasing the rate capability of the spectrometer; alternatively, the spectrometer might be moved to a higher-energy interaction region, either in fixed-target or collider mode, at the Tevatron, LHC, or SSC.

Contents

1 PHYSICS MOTIVATIONS

In the nineteen years since the discovery of charm and the fifteen since that of beauty, interest in heavy-quark decays has grown steadily. Several recent technical [1, 2, 3, 4, 5] and physics developments make this physics more accessible than ever to fixed-target experimentation at Fermilab:

- The success of E687 and E691/769/791 in amassing large samples of reconstructed charm events using Fermilab external beams and carrying out comprehensive studies of charm production and decay;
- The success of E789 in operating silicon vertex detectors at $> 50\,\mathrm{MHz}$ interaction rate [6] and in triggering on secondary vertices [7];
- The development of high-rate tracking devices for SSC experiments [8, 9];
- The growing feasibility of recording and analyzing extremely large data sets using commercially available data acquisition and computing equipment.

These developments lead us to propose a new spectrometer to take the study of heavy quarks to new levels of sensitivity. We envision an apparatus capable of studying $\sim 10^{14}$ interactions per fixed-target run, triggering on charm and beauty events with $10^{-3} - 10^{-4}$ trigger rejection against light-quark backgrounds, and fully reconstructing $\sim 10^7 - 10^8$ charm and $\sim 10^4$ beauty decays. A novel optical impact-parameter trigger [1], described in Section 3.6.1 and Appendix III, is key to achieving this performance.

As will be seen in Section 3, our proposed apparatus resembles a more compact version of the fixed-target beauty spectrometer proposed for internal-target operation at HERA [10]. That highly ambitious proposal aims to observe CP violation in the $B^0 \to J/\psi K_s$ mode with $\sim 10^9$ beauty events produced. We believe that before such a large effort is undertaken, the utility of such an approach should be demonstrated by taking a smaller, less costly step in sensitivity. This can be accomplished by designing for the 10^8-produced-event regime, as here proposed. As discussed above, such a sample corresponds to $\sim 10^4$ beauty decays fully reconstructed and a larger number partially reconstructed.

Since the spectrometer has similar acceptances for charm and for beauty, a large sample of charm decays will be amassed simultaneously with the beauty sample. The cross section times branching ratio for fully-reconstructable charm decays is $\sim 10^5$ times that for beauty. To bring the rate of recorded minimum-bias events down to acceptable levels necessitates a trigger which is 1 – 10% as efficient for charm as for beauty. Thus the fully-reconstructed charm sample will amount to some 10^7 to 10^8 decays.

1.1 Beauty physics goals

The study of b quarks is entering an advanced stage. Many general properties of the B system are known, such as: the existence of B_d^0 and B_s^0 mixing [11], limits on FCNC B

decays [12], initial estimates of the $B^{\pm}$, B_d^0, B_s^0, and Λ_b lifetimes [13], and the observation of decays that imply that $|V_{ub}| \neq 0$ [13]. However, several important issues remain, including

(i) The measurement of χ_s for $B_s^0 - \bar{B}_s^0$ mixing

(ii) Precision measurement of Λ_b, B_s^0 lifetimes

(iii) Search for FCNC processes $b \to s\gamma$ and $b \to s\mu^+\mu^-$

(iv) Measurement of interesting rare decays such as $B \to \pi\pi$, πK, etc.

(v) Detection of CP violation in B decays

We believe that some of these issues can be resolved using the approach proposed here. We next discuss these issues in more detail.

(i) Measurement of χ_s

While $B_s^0 - \bar{B}_s^0$ mixing is inferred from the measurements at $\bar{p}p$ colliders (UA1 [11], CDF [14]) and LEP (all 4 detectors) [13], the value of χ_s is at present unknown. The most likely value is between 8 and 24 and measures

$$\chi_s \propto \left|\frac{V_{td}}{V_{ts}}\right|^2,$$

a crucial ratio of the CKM matrix. These large values of χ_s can only be observed by measuring the mixing oscillations, and thus the proper time for each B_s^0 decay. It is also necessary to tag the initial beauty quantum number of the B_s^0. We are simulating two B_s^0 decay modes which appear promising:

$$\begin{aligned} \bar{B}_s^0 &\to D_s^+ + \ell + \bar{\nu} + X \\ &\hookrightarrow \phi\pi^+ \\ &\hookrightarrow K^+K^- \end{aligned}$$

$$\begin{aligned} \bar{B}_s^0 &\to D_s^+ + \ell + \bar{\nu} + X \\ &\hookrightarrow \bar{K}^{*0}K^+ \\ &\hookrightarrow K^-\pi^+ \end{aligned}$$

As shown in Section 2.2.2, these modes will provide substantial samples of partially-reconstructed events. However, undetected neutrals will induce smearing of the reconstructed decay vertex which could limit sensitivity at larger values of χ_s. There will also be smaller samples of fully-reconstructed events, for example:

$$\bar{B}_s^0 \rightarrow \quad D_s^+ + \pi^- \hookrightarrow \phi\pi^+ \text{ or } \bar{K}^{*0} K^+$$

$$\bar{B}_s^0 \rightarrow \quad D^0 + \bar{K}^{*0} \rightarrow K^-\pi^+K^-\pi^+$$

etc.

(ii) Precision Measurement of Λ_b and B_s^0 Lifetimes

For the charm system there is a large variation in the lifetimes. From LEP data [13] we already know that the same situation does not hold for the b-quark systems. Nevertheless, there could be variations at the level of 20%, and considerable precision can be obtained using the fixed-target experiment proposed here. A key element of this program is to identify B_s^0 decays as discussed before and Λ_b by the decay chains

$$\Lambda_b \rightarrow \quad \Lambda_c^+ + \ell^- + \bar{\nu} \hookrightarrow \Lambda^0 + \pi^+ \hookrightarrow p\pi^-$$

and

$$\Lambda_b \rightarrow \quad J/\psi + \Lambda \hookrightarrow \ell^+\ell^-$$

(iii) Search for FCNC Processes $b \rightarrow s\gamma$ and $b \rightarrow s\mu^+\mu^-$

While it is well known that tree-level Flavor-Changing Neutral Currents (FCNC) are not observed in the K system, the situation for heavy quarks is less certain. Currently the best limit comes from the UA1 experiment [12]:

$$BR\left(B \rightarrow \mu^+\mu^- X\right) \leq 5 \times 10^{-5}\,.$$

These processes probe small tree-level FCNC amplitudes, loop diagrams with a t-quark mass sensitivity, and possible SUSY contributions to FCNC (one of the few low-energy processes which could be sensitive to SUSY). The real- and virtual-photon processes also probe different matrix elements and Feynman diagrams (as shown by Mark Wise and colleagues at Caltech [15]): whereas the real-photon process probes states accessible only to a real photon, the virtual-photon states allow massive photons with arbitrary polarization. For example, the final states

$$B \rightarrow J/\psi + X$$

can be reached in this latter process, and interference with virtual loop digrams is expected [15, 16, 17].

The experimental signatures and backgrounds are quite different for the two processes. We discuss first $b \to \binom{s}{d} + \gamma$, which would be detected as

$$\begin{aligned} & B \to X_s + \gamma \\ \text{and} \quad & B \to X_d + \gamma . \end{aligned}$$

The expected branching ratios of these processes are $\sim 10^{-4}$ and $\sim 10^{-5}$, respectively [16]. Of course there will also be exclusive processes like

$$\begin{aligned} & B \to K^* + \gamma \\ \text{and} \quad & B \to \rho + \gamma \end{aligned}$$

which might be detected at a lower branching-ratio level. The detection of these processes in hadroproduction is quite challenging due to the large number of π^0's in each event, but it may be possible given sufficiently good electromagnetic calorimetry and photon isolation techniques. A recent calculation by Ali *et al.* [18] suggests that $B \to K_2^*(1430)\gamma$ could make up a substantial fraction (17 – 37%) of these decays, providing an additional signature considerably cleaner than the inclusive-γ spectrum.

The detailed study of $B \to X + \gamma$ is very important for our understanding of the Standard Model as applied to B decays and the search for physics beyond the Standard Model. This process is very sensitive to the possible existence of FCNC at tree level and to such extensions of the Standard Model as Supersymmetry [19]. It also has some slight sensitivity to the t-quark mass. The current experimental limit on $B \to X\gamma$ is 8.4×10^{-4} from CLEO II [20].

In contrast, the process $B \to X\mu^+\mu^-$ is highly sensitive to the t-quark mass as well as to the existence of tree-level FCNC. While UA1 (and presumably CDF) have searched for this process in a tiny region of phase space at the high-mass end of the $\mu\mu$ mass spectrum ($\sim 5\,\mathrm{GeV}$), the proposed experiment will be sensitive to masses down to or below the $\psi/\psi\prime$ mass region [15, 17].

(iv) Measurement of interesting rare decays

The decay $B^0 \to \pi^+\pi^-$ is of interest both because of its large predicted CP asymmetry in the Standard Model [21, 22] and because its branching ratio is proportional to $|V_{ub}|^2$ [21]:

$$BR(B^0 \to \pi^+\pi^-) \approx 2 \times 10^{-3} \left| \frac{V_{ub}}{V_{cb}} \right|^2 .$$

It has not yet been observed; the best experimental limit comes from CLEO and is $< 4.8 \times 10^{-5}$ at 90% confidence level [13]. Other charmless dihadronic beauty decays are likely to be observed simultaneously with $B^0 \to \pi^+\pi^-$: $B^0 \to \pi^\pm K^\mp$, $K^\pm K^\mp$, $p\bar{p}$, $\Lambda_b \to p\pi^-$, etc. The rates of these decays are of interest in that their comparison with

$\pi^+\pi^-$ yields information about the role of penguin diagrams, final-state interactions, and baryonic effects in beauty decay.

(v) Detection of CP violation in B decays

Observation of CP violation in B-meson decay is one of the most sought-after goals of contemporary high energy physics. Much attention [10, 21, 23] has been given to a few rare, low-multiplicity decay modes with large expected CP-violating asymmetries which in principle can test the Kobayashi-Maskawa model for CP violation by overconstraining the "unitarity triangle." These include the decays $B_d \to J/\psi K_s$, $B_d \to \pi^+\pi^-$, and $B_s \to \rho^0 K_s$, two of which have yet to be observed. The first of these modes has an observable branching ratio of 2×10^{-5}, and models suggest that the last two could have observable branching ratios of order 10^{-5} and 10^{-6}, respectively [21, 24]. Thus in the Standard Model observation of CP violation in these modes will probably require the production of at least 10^9 B mesons in an experiment configured to have large acceptance and good tagging capability. At the 10^8-event level, useful investigations of backgrounds and tagging strategies can be carried out. It is also possible that physics beyond the Standard Model (or favorable parameter values within the Standard Model) could lead to observable CP asymmetries at this level; for example, Gronau [22] has recently suggested that penguin effects in $B^0 \to \pi^+\pi^-$ could lead to a CP asymmetry as large as 40%, possibly observable in the proposed experiment (see Section 2.2.3).

Many B-tagging strategies seem potentially useful: tagging with high-p_t leptons or with moderate-p_t kaons; tagging with those particles but also imposing impact-parameter requirements at the primary vertex; tagging with partially-reconstructed decays; and tagging with fully-reconstructed decays. These strategies will provide various levels of purity and efficiency which can be approximately predicted by Monte-Carlo simulation. An experimental test (such as that proposed here) is required before their utility can be assessed with confidence.

In addition to the modes discussed above, Dunietz and others [25] have emphasized the role of charged-B and self-tagging neutral-B modes in constraining the CKM matrix. These may be accessible with somewhat fewer produced B's than are required for the tagged modes. They may also have greater potential for determining the CKM angle γ than does the $B_s \to \rho^0 K_s$ decay [25]. Since some of the self-tagging modes include final-state π^0's, good electromagnetic calorimetry might significantly enhance the ability to study CP violation.

1.2 Charm physics goals

Previous experiments have reached the 10^5-reconstructed-charm level, and in the next run E831 is expected to reconstruct $\sim 10^6$ charm events. We propose a further increase in sensitivity by one to two orders of magnitude. At such sensitivities the following physics issues could become accessible:

(i) Second-order weak interactions ($D^0 - \bar{D}^0$ mixing) and CP violation in charm meson decays [26]

(ii) Pure leptonic decays of D^+ and D_s, yielding f_D and f_{D_s}

(iii) High-statistics study of semileptonic decays, yielding more precise mesurements of the CKM matrix

(iv) Rare D^0, D^+, and D_s decays measuring radiative and hadronic penguins and searches for new physics (decays outside the Standard Model); measurement of doubly-Cabibbo-suppressed decays and beyond

(v) Measuring lifetimes to better than 1% and absolute branching ratios (using the double-tagged method pioneered by ACCMOR [27])

(vi) Charmed baryons

(vii) Search for FCNC charm decays such as $D \to \mu^+\mu^- X$ and $D^0 \to \mu^+\mu^-$ [28]

We next consider a few of these topics in greater detail.

(i) <u>$D^0 - \bar{D}^0$ Mixing</u>

$D^0 - \bar{D}^0$ mixing would be characterized by a mass splitting ΔM_D and width difference $\Delta\Gamma$, and parametrized in the usual way by $\chi_D = \Delta M_D/\Gamma$ and $y_D = \Delta\Gamma/2\Gamma$. As in B^0 mixing we expect $\Delta\Gamma/2\Gamma << 1$. The mixing can be detected by observing events with

$$\begin{array}{ccc} D^0\bar{D}^0 & & \bar{D}^0 D^0 \\ \quad \hookrightarrow D^0 & \text{or} & \quad \hookrightarrow \bar{D}^0 \end{array}$$

through same-sign dimuon and Cabibbo-forbidden processes. For example, one may detect

$$r_D = \frac{B\left[D^0 \to \bar{D}^0 \to \bar{f}\right]}{B\left[D^0 \to f\right]} \simeq \frac{\chi_D^2}{2}.$$

Calculations by Wolfenstein [26] give $r_D < 10^{-5}$ in the Standard Model, although calculations which attempt to take into account final-state interactions between the light quarks predict a value closer to 5×10^{-4} [29]. The current experimental limit is approximately 4×10^{-3} [30]. New physics could give larger values of r_D, thus this channel is important to the search for physics beyond the Standard Model. To detect $D^0 - \bar{D}^0$ mixing to the level of 10^{-6} requires the study of $>10^6$ double-semileptonic decays. A careful study of various backgrounds is required to determine whether this level of signal can be extracted from the data!

A second technique is to use the decay $D^{*+} \to D^0\pi^+$ to tag the flavor of the D^0;

then the D^0 can be fully reconstructed through the large decay modes $K^-\pi^+$ and $K^-\pi^+\pi^+\pi^-$. Essentially, a non-mixed decay is signalled through the opposite sign of the soft pion and the kaon in the D decay. $D^0 - \bar{D}^0$ mixing (or a doubly Cabibbo-suppressed decay) would be indicated by a soft pion and a kaon of the same sign. The ratio of the same-sign and opposite-sign rates is a function of integrated proper time if mixing is occurring; this allows sorting out of mixing from doubly Cabibbo-suppressed decays. It should be possible to obtain a limit near 1×10^{-4} using this technique.

(iii) Semileptonic Decays

This is an extremely rich area of charm physics: studies of semileptonic decays permit the determination of several parameters of the Standard Model. Currently-observed semileptonic decay modes for the D^0 are listed in Table 1.1.

TABLE 1.1 Selected charm semileptonic branching ratios

Decay Mode	BR (%)	Exp't
$D^0 \to K^- e^+ \nu_e$	$3.8 \pm 0.5 \pm 0.6$	E691 [31]
	$3.9 \pm 0.2 \pm 0.7$	ARGUS [32]
	$3.8 \pm 0.3 \pm 0.6$	CLEO [33]
	$3.4 \pm 0.5 \pm 0.4$	Mark III [34]
$D^0 \to K^- \mu^+ \nu_\mu$	$2.5 \pm 0.4 \pm 0.5$	E653 [35]
$D^0 \to \pi^- e^+ \nu_e$	$0.39^{+0.23}_{-0.11} \pm 0.04$	Mark III [36]

Branching-ratio measurements of $D^+ \to K^* l\nu$ and $D^0 \to Kl\nu$ should permit determination of $|V_{cs}|$ to about 1%. We can then extract the form factor using the world-averaged D^0 lifetime and the absolute branching fraction from Mark III [36]. This form factor can be compared to that found in 4-body hadronic decays of the D mesons [37]. It is also possible to measure $|V_{cs}/V_{cd}|$ in the proposed experiment by using the branching ratio of $D^0 \to \pi^- e^+ \nu_e$:

$$\left|\frac{V_{cs}}{V_{cd}}\right|^2 = \frac{\Gamma(D^0 \to \pi^- e^+ \nu_e)}{\Gamma(D^0 \to K^- e^+ \nu_e)} \times \left[\frac{f_+^K(0)}{f_+^\pi(0)}\right]^2 .$$

The dominant source of error in this measurement in likely to be the error of the form factors, since the statistical error will likely be $< 1\%$.

Relative branching ratios and form factors can also be extracted for the D^+ and D_s mesons, as well as the polarization of the W for all meson decays. With the sample sizes expected it should also be possible to study interference effects between various decays involving resonances, and we should be able to study semileptonic decays of charmed baryons in detail.

(iv) Doubly Cabibbo-suppressed decays

Doubly Cabibbo-suppressed decays (DCSD) of charm states can be most straightfor-

wardly addressed using the D^+, since there is then no possibility of confusion with $D^0 - \bar{D}^0$ mixing. Examples of decay modes are $D^+ \to K^+\pi^-\pi^-$ and $D^+ \to K^+K^+K^-$. The second mode has possibly been seen by E691 ($D^+ \to \phi K^+$); if their $\sim 2\sigma$ signal is correct we should expect to see several thousand in the proposed experiment. We expect the DCSD rate to be down relative to the Cabibbo-allowed mode by $\tan^4\theta_c \sim 3 \times 10^{-3}$, which is well below the E691 observation, however even this lower value implies hundreds of reconstructed decays in our apparatus.

(vi) Charmed Baryons

Much less is known about the baryon sector of charm. This has to do in large part with the smaller production cross sections and short lifetimes of the charmed baryons. Most charmed-baryon decays involve hyperons, which impose special requirements on the apparatus in order to detect them. Our proposed spectrometer has about 2 meters of decay space between the target and the downstream fiber tracker. This should allow good acceptance for both neutral (Λ^0) and charged ($\Sigma^\pm$) hyperon decays (even though the decays may occur inside the magnet [38]). The RICH detector will offer good particle identification for the proton produced in the decay.

(vii) Search for FCNC decays

The search for charm-changing neutral currents can be carried out via

$$\begin{aligned} & D^0 \to \quad \mu^+\mu^- \\ \text{and} \quad & D^0 \to \quad \mu^+\mu^- X \end{aligned}$$

Both of these processes are expected to have very small branching ratios in the standard model ($\leq 10^{-16}$ for $D^0 \to \mu^+\mu^-$), and thus provide a window for physics beyond the Standard Model [28]. The search for $D \to \mu^+\mu^- X$ is similar to that for $B \to \mu^+\mu^- X$ except that the long-range pole in the D^0 case is the ϕ. Thus, it is important to search for this process in the low-mass range, $\sim 1\,\text{GeV}$ dilepton mass.

2 PROPOSED MEASUREMENTS

The proposed apparatus (see Section 3) is rather general and is expected to address a wide range of physics. In this section we consider several illustrative examples.

2.1 Predicted yields

The cross section for production of D mesons by 800 GeV protons has been measured by E653 [39] and E743 [40] using emulsion and hydrogen targets, respectively: E653 finds $(76 \pm 9 \pm 27)\,\mu$b (assuming $\sigma_D \propto A^1$) and E743 $(48^{+10}_{-8} \pm 12)\,\mu$b. (Preliminary results from E789 are consistent with these values.) Averaging the two, we find a total charm cross section of $(56 \pm 8 \pm 14)\,\mu$b, neglecting the small contribution due to D_s and charmed baryons. Since these are individual meson cross sections, the $c\bar{c}$ cross section is $\approx 1/2$ this value. Precise measurements of the A-dependence for J/ψ production are available from E772 [41], giving $\sigma_{J/\psi} \propto A^{0.92\pm0.01}$. A preliminary D A-dependence measurement from E789 gives $\sigma_D \propto A^{0.90\pm0.04}$, consistent with the E772 J/ψ result. Given the cross-section and A-dependence uncertainties, it clear that charm yields are known to about $\pm(25-50)\%$. Thus the uncertainty in the number of charm events recorded will be dominated by the uncertainty in trigger efficiency.

While the $b\bar{b}$ cross section in 800-GeV hadroproduction is not precisely known, based on $O(\alpha_s^3)$ QCD calculations [42] Berger [43] has predicted it to lie in the range 9–19 nb; we use 10 nb in this proposal. (Preliminary results from E789 are consistent with this value.) The A-dependence of beauty production is unknown but generally assumed to be linear. E772 [44] has measured $\sigma_\Upsilon \propto A^{0.96\pm0.01}$. We therefore assume (conservatively) the same A-dependence for open-beauty production.

We assume a 50 MHz interaction rate for a canonical fixed-target run of 3×10^6 seconds of beam, giving 1.5×10^{14} inelastic interactions. Table 2.1 estimates the resulting yields of charm and beauty events.

TABLE 2.1 Expected yields of heavy-quark events

	charm	beauty
$\sigma_{q\bar{q}}$	28 μb	10 nb
A-dependence enhancement factor*	3.0	3.7
events/interaction	2.6×10^{-3}	10^{-6}
total events produced	4×10^{11}	1.7×10^8

* assuming gold target and $\sigma_{c\bar{c}} \propto A^{0.92}$, $\sigma_{b\bar{b}} \propto A^{0.96}$

In estimating yields of reconstructed decays, we assume for simplicity that the geometrical acceptance for an n-prong final state is given by $(0.7)^n$. Appendix I shows that this is likely to be a slight underestimate for beauty and a slight overestimate for charm, but these errors are small compared to the uncertainties in the beauty cross section and charm trigger efficiency. Based in part on experience in E789, we assume a 20% trigger efficiency for beauty and a reconstruction efficiency of 0.9/prong. For modes containing a final-state π^0 or missing neutrino, we reduce the reconstruction efficiency to account for additional kinematic and calorimetric cuts.

2.2 Beauty measurements

2.2.1 $b \to s\gamma$

The predicted inclusive branching ratio, $\sim$ a few $\times 10^{-4}$ [16], implies several $\times\, 10^4$ $b \to s\gamma$ events produced, of which $10^3 \sim 10^4$ are expected to satisfy the acceptance and the trigger. The γ spectrum [16] in the B rest frame is shown in Figure 2.1; as one expects it peaks near $1/2$ the mass of the the B. The crucial difficulty in detecting the signal is the substantial background of photons due to π^0 decay. Preliminary Monte-Carlo simulations (see Appendix I) suggest that with good electromagnetic calorimetry, background suppression adequate for the inclusive-γ signal to be discerned is possible. Confirming evidence should come from exclusive modes such as $B \to K^*\gamma$, of which there should be several thousand produced events and $10^2 \sim 10^3$ reconstructed.

2.2.2 B_s mixing

The LEP experiments have measured [13] the following product of hadronization and branching ratios:

$$BR(b \to \bar{B}_s) \times BR(\bar{B}_s \to D_s^+ X \ell^- \bar{\nu}) = (1.59 \pm 0.42)\% .$$

Thus, including the flavor-conjugate (B_s) mode, we expect to produce 0.032 ± 0.008 such decays per $b\bar{b}$ event. Table 2.2 gives expected sensitivities in the most copious B_s modes, and Table 2.3 gives sensitivities in selected fully-reconstructed modes. (Table 2.3 is based on the assumption $BR(b \to \bar{B}_s) = 0.125$.) Applying the tagging efficiencies discussed below (see Section 2.2.3), we estimate 2,500 and 400 tagged B_s or $\bar{B}_s$ events in the partially- and fully-reconstructed samples. Simulations are in progress to estimate the resulting χ_s sensitivity.

TABLE 2.2 Expected yields of $\bar{B}_s \to D_s^+ \ell^- \bar{\nu} X \to K^+K^-\pi^+\ell^-\nu X$ and $B_s \to D_s^- \ell^+ \nu X \to K^-K^+\pi^-\ell^+\bar{\nu}X$

	$D_s \to \phi\pi$	$D_s \to K^{*0}K$
$b\bar{b}$ events produced	1.7×10^8	1.7×10^8
$(D_s^{\pm} X \ell\nu)$ per $b\bar{b}$ event	0.032	0.032
$BR(D_s \to KK\pi)$	0.0137	0.0162
geometrical acceptance	0.24	0.24
trigger efficiency*	0.2	0.2
reconstruction efficiency*	0.5	0.5
number of events $(\bar{B}_s + B_s)$	1800	2000

* note that vertex cuts are made both on- and off-line, thus vertexing efficiency is included in both trigger and reconstruction efficiencies.

TABLE 2.3 Expected yields in selected fully-reconstructed $B_s \to D$ modes

mode:	$D_s^-\pi^+$	$\vdash \cdots$	$\cdots \bar{D}^0 K^{*0} \cdots$	$\cdots \dashv$
final state:	$K^+K^-\pi^-\pi^+$	$K^+\pi^-K^+\pi^-$	$K^+\pi^-\pi^0K^+\pi^-$	$K^+\pi^-\pi^-\pi^+K^+\pi^-$
BR*	1.5×10^{-4}	1.3×10^{-4}	4×10^{-4}	3×10^{-4}
geometrical acceptance†	0.24	0.24	0.12	0.12
trigger efficiency	0.2	0.2	0.2	0.2
reconstruction efficiency†	0.6	0.6	0.4	0.4
number of events $(\bar{B}_s + B_s)$	180	160	160	120

* B_s branching ratios are estimated from corresponding B_u and B_d modes.

2.2.3 Charmless beauty decays

These are of interest for their sensitivity to $|V_{ub}|$, final-state interactions, and penguin diagrams; they may also exhibit large CP asymmetries [21, 22]. We take $B^0 \to \pi^+\pi^-$ as an example. Using the best current estimate [13] for $|V_{ub}/V_{cb}| \approx 0.07$, one finds

$$BR(B^0 \to \pi^+\pi^-) \approx 1 \times 10^{-5},$$

leading to the sensitivity prediction of Table 2.4. We note that the CLEO and ARGUS data can accomodate a range of $|V_{ub}/V_{cb}|$ from 0.05 to 0.15 [13], giving a branching-ratio range $(0.5 - 5) \times 10^{-5}$. Other charmless two-prong modes of B^0 ($\pi^{\pm}K^{\mp}$, K^+K^-, and $p\bar{p}$) will have similar acceptances and efficiencies as $\pi^+\pi^-$, but their branching ratios are even more uncertain, due to their increased sensitivities to penguins and final-state interactions [21]. There will also be significant sensitivity to charmless decays of B_s, $B^{\pm}$, and beautiful baryons.

TABLE 2.4 Expected yield of $B^0 \to \pi^+\pi^-$

$b\bar{b}$ events produced	1.7×10^8
hadronization fraction $b\bar{b} \to b\bar{d}$ or $\bar{b}d$	0.75
$BR(B^0 \to \pi^+\pi^-)$*	1×10^{-5}
geometrical acceptance	0.5
trigger efficiency†	0.2
reconstruction efficiency†	0.8
number of events	100

* assuming $|V_{ub}/V_{cb}| = 0.07$

† note that vertex cuts are made both on- and off-line, thus vertexing efficiency is included in both trigger and reconstruction efficiencies.

Table 2.5 indicates how many reconstructed $B^0 \to \pi^+\pi^-$ events are likely to be flavor-tagged by a lepton or a charged kaon. Our estimates of tagging efficiency and dilution follow Albrecht *et al.* [10]. The numbers of tagged events are small, and given the dilution factors, even if the CP asymmetry is as large as 40% it will be observed only at the $\approx$1.5-σ level. Sensitivity could be improved if further tagging strategies or means to ameliorate the dilution factors can be devised, or if the yield of reconstructed events is larger than estimated here.

TABLE 2.5 Expected yield of tagged $B^0 \to \pi^+\pi^-$

	lepton tag	kaon tag
reconstructed events	100	100
tagging efficiency	0.15	0.52
dilution factor	0.52	0.36
number of tagged events	15	50

Another potentially interesting charmless mode is $B^0 \to p\bar{p}\pi^+\pi^-$, which may have been

observed by ARGUS [45]. While with better sensitivity CLEO failed to observe it [46], the ARGUS and CLEO results are barely consistent if the actual branching ratio is $\approx 1 \times 10^{-4}$, in which case several hundred events would be expected in the proposed experiment.

2.2.4 Self-tagging CP-violating modes

Dunietz [25] has emphasized a class of self-tagging charged-B decay modes which may exhibit observable CP asymmetries. We consider the decays $B^- \to D^0 + X^-$ and $B^- \to \bar{D}^0 + X^-$. The first occurs via a $b \to c$ conversion and the second via $b \to u$. If the $D^0 (\bar{D}^0)$ is observed in K^+K^-, $\pi^+\pi^-$, or another mode accessible to both D^0 and $\bar{D}^0$, then the D and $\bar{D}$ final states are indistinguishable and should interfere, leading to the CP violation $BR(B^- \to D^0 + X^-) \neq BR(B^+ \to D^0 + X^+)$. The final-state phases in these modes are rather uncertain, but Dunietz estimates Standard-Model CP asymmetries in the range 1 – 10% [25]. Table 2.6 estimates the sensitivity in a few of these modes. The reconstruction efficiencies given are only educated guesses at this point; detailed simulations are required to refine them further. However, the possibility of useful CP sensitivity in these modes is evident: a 10% asymmetry would be observed with a significance of ≈ 3 standard deviations.

TABLE 2.6 Expected yields in selected $B^\pm \to D^0 (\bar{D}^0) + X^\pm$ modes

$B^- \to D^0(\bar{D}^0) + X$, where $X =$ $\hookrightarrow K^+K^-$ or $\pi^+\pi^-$	$\ell^-\bar{\nu}$	π^-	$\pi^+\pi^-\pi^-$	ρ^-
BR*	9.8×10^{-5}	2.0×10^{-5}	5.0×10^{-5}	6.3×10^{-5}
geometrical acceptance	0.34	0.34	0.17	0.17
trigger efficiency	0.2	0.2	0.2	0.2
reconstruction efficiency	0.5	0.7	0.6	0.5
number of events $(B^- + B^+)$	400	100	100	100

* branching ratios are averages of B^+ and B^0 branching ratios from the **Review of Particle Properties**, Phys. Rev. **D45**, Part 2 (1992).

2.2.5 Fully reconstructed $B \to D$ decays

Large numbers of beauty decays to final states including D mesons will be reconstructed. These may be used for precise determination of lifetimes and masses. Approximately 10% of neutral and charged D decays are visible in fully reconstructed modes ($K\pi$, $K\pi\pi$, $K3\pi$,...). Using this approximation, Tables 2.7 and 2.8 estimate the expected numbers of events in representative charged and neutral modes. These samples could also be used to search for

B-meson excited states, which would be signalled by the presence of soft pions or photons collinear with the B. Since the proposed target represents $\approx 1/3$ of a radiation length on average, a significant fraction of these photons will emerge as electron-positron pairs, which will be measured accurately by the magnetic spectrometer, and an additional sample of unconverted photons will be measured by the calorimeter.

TABLE 2.7 Expected yields in selected fully-reconstructed $B^{\pm} \rightarrow D$ modes

mode:	$D^0\pi^-$	$D^0\pi^+\pi^-\pi^-$	$D^0\rho^-$
BR*	3×10^{-4}	9×10^{-4}	1×10^{-3}
geometrical acceptance†	0.34	0.17	0.17
trigger efficiency	0.2	0.2	0.2
reconstruction efficiency†	0.7	0.6	0.5
number of events $(B^- + B^+)$	2000	2000	2000

* branching ratios are averages of B^+ and B^0 branching ratios from the **Review of Particle Properties**, Phys. Rev. **D45**, Part 2 (1992), scaled by 0.1 to account for D^0 reconstruction.

† acceptances and reconstruction efficiencies are estimated for 2-prong decay of the D^0.

TABLE 2.8 Expected yields in selected fully-reconstructed $B^0 \rightarrow D$ modes

mode:	$D^+\pi^-$	$D^+\pi^+\pi^-\pi^-$	$D^+\rho^-$
BR*	3×10^{-4}	9×10^{-4}	1×10^{-3}
geometrical acceptance†	0.24	0.12	0.12
trigger efficiency	0.2	0.2	0.2
reconstruction efficiency†	0.6	0.5	0.4
number of events $(B^- + B^+)$	1000	1000	1000

* branching ratios are averages of B^+ and B^0 branching ratios from the **Review of Particle Properties**, Phys. Rev. **D45**, Part 2 (1992), scaled by 0.1 to account for $D^{\pm}$ reconstruction.

† acceptances and reconstruction efficiencies are estimated for 3-prong decay of the $D^{\pm}$.

2.2.6 Partially reconstructed beauty decays

Since essentially 100% of beauty decays produce a D meson, there will be a very large number of partially reconstructed decays $B \rightarrow D + X$. These will determine the average beauty lifetime to high precision. For rare modes such as $B^0 \rightarrow \pi^+\pi^-$ and $B \rightarrow K^*\gamma$, requiring an additional partially-reconstructed B in the event could be a good strategy for reducing non-beauty background.

2.3 Charm measurements

More detailed simulations than have so far been completed are required to establish the geometrical acceptance, the efficiency of each level of our proposed vertex trigger, and the off-line reconstruction efficiency for each charm decay of interest. As a preliminary estimate we use an acceptance of 0.7/prong. As mentioned in Section 1, we expect a vertex trigger efficiency in the range $(0.2 - 2)\%$ (i.e. $(1 - 10)\%$ of that estimated for beauty); in the tables which follow, we have used 0.2%. We base our reconstruction efficiencies on those of E687 and E791. We include in this section two examples of our projected charm sensitivity based on these preliminary efficiency and acceptance estimates.

2.3.1 Semileptonic charm decays

Expected yields of D^0 semileptonic decays are indicated in Table 2.9.

TABLE 2.9 Semileptonic D^0 yields

Decay Channel	BR (%)	Events
$K^-l^+\nu$	3.4	10^5
$\pi^-l^+\nu$	0.4	10^4
$K^{*-}l^+\nu$	6.2	10^5
$\rho^-l^+\nu$	0.4	10^4

2.3.2 Charmed-baryon decays

Charmed-baryon yields should be approximately 1% of the meson yields. This gives a Λ_c sample of order $10^5 - 10^6$ events; the Ξ_c and Ω_c should be down from this by another factor of 10 – 50. With samples of this size it will be possible fully to study the resonant structure of the 3- and 4-body decays of the Λ_c and to determine to what extent 2-body decays occur in the baryon sector. Table 2.10 summarizes expected yields for some interesting decay modes of charmed baryons. The spectroscopy of charmed baryons is largely unexplored; we expect to observe doubly-charmed baryons as well as charmed-baryon resonances!

TABLE 2.10 Estimated Yields for Selected Charmed Baryon Decays

Decay Channel	Events
$\Lambda_c \rightarrow pK^-\pi^+$	10^5
$\Lambda_c \rightarrow pK_s\pi^+\pi^-$	3×10^4
$\Lambda_c \rightarrow p\pi^+\pi^-$	10^3
$\Xi_c^0 \rightarrow \Xi^-\pi^+$	2×10^3
$\Xi_c^+ \rightarrow \Xi^-\pi^+\pi^+$	2×10^3
$\Omega_c^0 \rightarrow \Omega^-\pi^+$	10^3

3 APPARATUS DESIGN

3.1 General considerations

We aim to maintain the high interaction-rate capability ($\approx$1 interaction per accelerator RF-bucket, or 5×10^7 interactions/s) demonstrated in E789 while increasing the solid-angle coverage (and hence beauty acceptance) substantially. At 800 GeV, the central 3 units of rapidity contain some 70% of produced particles. Monte-Carlo studies (see Appendix I) confirm that geometrical acceptance of $\approx(0.7)^n$ can be achieved for n-prong heavy-quark decays by instrumenting such a rapidity range. (In laboratory polar angle, this corresponds to approximately 8 to 150 mr.)

Figure 3.1 shows a typical event from E789, obtained at an interaction rate of 50 MHz. The hit density in the silicon detectors ($\approx$20 hits per plane on average) is seen to be quite tractable for pattern recognition. Figure 3.2 shows the transverse position resolution achieved. Figure 3.3 shows the observed dimuon mass distributions for events with reconstructed vertex upstream, inside, and downstream of the target; a clear $B \rightarrow J/\psi$ signal is evident in the downstream-vertex sample.

Figure 3.4 depicts the conceptual design of the proposed spectrometer. As in E789, the central beam hole permits operation at interaction rates up to 50 MHz. The choice of detector technology at each position in the spectrometer is driven by considerations of rate, coverage, resolution, and radiation damage.

3.2 Silicon detectors

The needed decay-vertex resolution dictates the use of silicon detectors near the target. These could be microstrip detectors, or the pixel detectors now under development by several groups [47]. Compared to strip detectors, pixel detectors could confer great benefits in pattern-recognition capability, radiation hardness, and cost [48, 49], but no existing prototype has sufficient speed or radiation hardness for the proposed experiment. Should high-speed radiation-hard pixel detectors become available on the needed time scale, we will revise our spectrometer design to make use of them. For the present, we present below a design based on strips.

The silicon detectors are arranged in two arms, one above and one below the beam. Their minimum transverse distance from the beam is driven by the maximum allowable radiation fluence, which we estimate to be $\approx$ 10 MRad [50, 10] if the detectors are to remain functional for an entire fixed-target run. For the desired sensitivity of 10^{14} interactions, this requirement leads to a $\approx$6 mm minimum transverse distance from the beam, which is compatible with the desired angular coverage if the silicon detectors extend to $\approx$1.3 m from the target.

Note that in this design, the tracks of large-angle secondaries are measured by the silicon planes close to the target, while those of small-angle secondaries are measured far from the target. To maintain the same impact-parameter resolution at the target for all angles, the

detector separation scales geometrically. With this arrangement we find an average of 12 silicon-detector hits per track, approximately independent of angle, in the vertical angular range 8 to 150 mr. Since track momentum tends to scale as $1/\theta$, the multiple-scattering contribution to the vertex measurement error is also approximately angle-independent. In any given plane the hit density is no greater than that of the most upstream silicon planes in E789, thus we are confident that the tracks can be well reconstructed. Also the radiation damage will be similar to that encountered in E789. Simulations are in progress to verify the pattern-recognition efficacy of the proposed configuration. The large number of measurements per track should substantially improve trackfinding compared to E789 experience.

We propose to employ two new silicon-microstrip detector configurations made from double-sided 4" wafers (see Table 3.1). These feature small-angle (10°) stereo, thus each double-sided plane measures both the bend view (y) and a u ($+10°$) or (by 180° rotation) v ($-10°$) view. As in E789, holes are provided in the fanout circuit boards above and below the detector chips; these allow large-angle secondaries measured by the upstream planes to pass above and below the downstream planes with minimal scattering. Also as in E789, the detectors are mounted in a helium-filled box which provides electrical shielding, minimizes scattering, and permits cooled operation of the detectors to alleviate radiation-damage effects. The preamplifiers, mounted far from the beam at the edges of the fanout boards, receive much lower irradiation than the detectors and experience negligible radiation damage.

TABLE 3.1 Silicon-Microstrip Detector Configuration

plane	z (cm)	$\lvert x_{max}\rvert$ (cm)	$\lvert y_{min}\rvert$ (cm)	$\lvert y_{max}\rvert$ (cm)	channels/arm
ys1/us1	16.0	4.4	0.64	2.56	384/384
ys2/vs2	18.8	4.4	0.64	3.20	512/512
ys3/us3	22.0	4.4	0.64	3.20	512/512
ys4/vs4	25.9	4.4	0.64	3.20	512/512
ys5/us5	30.3	4.4	0.64	1.92	256/256
ys6/vs6	35.6	4.4	0.64	1.92	256/256
ys7/us7	41.8	4.4	0.64	1.92	256/256
ys8/vs8	49.0	4.4	0.64	1.92	256/256
ys9/us9	57.5	4.4	0.64	1.92	256/256
ys10/vs10	67.5	4.4	0.64	1.92	256/256
ys11/us11	79.2	4.4	0.64	1.92	256/256
ys12/vs12	93.0	4.4	0.64	1.92	256/256
ys13/us13	108.0	4.4	0.64	1.92	256/256
ys14/vs14	118.0	4.4	0.64	1.92	256/256
ys15/us15	128.0	4.4	0.64	1.92	256/256
Total channel count:					9,472 up + 9,472 down = 18,944

3.3 Analyzing magnet

A small magnet (p_t kick $\approx$0.5 GeV) suffices for $< 1\%$ r.m.s. mass resolution. A modified "40D48" magnet previously used by E711 is available and appears suitable (as shown in Figure 3.4). To achieve the desired momentum resolution, we propose to increase the magnet's p_t kick by shimming its pole pieces to a taper matching that of the instrumented aperture.

3.4 Downstream tracking detectors

Downstream of the analyzing magnet, the aperture is necessarily substantially larger than upstream, due to the divergence of the large-angle secondaries. Thus a detector technology is needed which can cover a large ($> 1\,\mathrm{m}^2$) area but also cope with high rates. The most likely choice appears to be scintillating fibers read out with visible-light photon counters (VLPCs) [8, 9], which have lately received substantial development support from the SSC. This is also the technology of choice for tracking in the D0 upgrade, and we expect its feasibility for large-scale application to be demonstrated by the D0 "3000-channel test" under preparation at Fermilab. Our collaboration includes members of the SDC fiber tracking

group, and we are also following closely the D0-upgrade R&D effort. Alternate choices for these detectors include gas microstrip [51] and small-cell cathode-pad chambers [52]; we judge these technologies to be at a less advanced stage of development, but they are fallback options should unanticipated problems be encountered with fiber tracking.

The scintillating fibers will be of the "multiclad" type lately developed by the Kuraray Co. for SDC. Recent test results obtained at Fermilab with such fibers show that over 60% more photons are captured and transmitted through them compared to single-clad fibers of the same type [53]. Each fiber will consist of a 740-μm-diameter polystyrene core doped with 1500 ppm of 3-hydroxyflavone (3HF) and 1% of p-terphenyl (PTP), with a two-stage step-index cladding. The total diameter of the fiber will be 800 μm, with each cladding layer of 15 μm thickness. As detailed below, we anticipate a minimum of $\approx$5 photoelectrons detected per minimum-ionizing particle, thus ensuring good detection efficiency. Tests of 3HF+PTP-doped polystyrene fibers show that they are radiation resistant beyond 10 MRad fluence [54].

As shown in Table 3.2, we propose to build five scintillating-fiber stations. The fiber planes will be organized in doublets, with half-cell stagger of the planes in each doublet to ensure good efficiency at the boundaries between adjacent fibers and to improve the position resolution. Each station will comprise three fiber-plane doublets measuring y, u, and v. Within each fiber plane the spacing is 800 μm. Each fiber is up to 3 m in length and is coupled to 3 m of clear optical fiber to carry the photons to the photodetectors. We believe that VLPCs will serve well as the photodetectors. Rockwell International Science Center has already produced [55] over 50,000 channels of VLPCs for UCLA, the SSC Laboratory, and Fermilab, of which several hundred have so far been packaged and tested. Since VLPC development is an ongoing process, devices from various production runs have differed in quantum efficiency and in dark-count rate. The latest batch fabricated [55] (30 wafers containing 45,000 channels in total) have quantum efficiencies ranging from 45 to 85% for the $\approx$530-nm-wavelength photons produced from 3HF+PTP scintillating fibers (see Figure 3.5) [56]. Much of the parameter variation within a batch is attributed to low levels of contamination in the epitaxy process, due to Rockwell's use of their device-development epitaxial reactor rather than their production reactor; they are confident of achieving $>$ 65% quantum efficiency routinely in batches fabricated using their production reactor, in which cleanliness is more stringently controlled. Nevertheless, we have designed our tracking planes based on the conservative assumption of 45% quantum efficiency. Rate capability of 30 MHz/pixel has been demonstrated [57]. The use and operation of VLPCs is by now well understood after several rounds of cosmic-ray [8, 9] and beam [58] tests. The UCLA/Fermilab/Rockwell test units have operated successfully with a number of installed channels in the hundreds. Work is in progress at Fermilab to design cryogenic systems for D0 fiber tracking to maintain the VLPCs at the desired temperature, and we anticipate using this design as well.

TABLE 3.2 Scintillating-Fiber Detector Configuration

plane	z (cm)	$\lvert x_{max}\rvert$ (cm)	$\lvert y_{min}\rvert$ (cm)	$\lvert y_{max}\rvert$ (cm)	channels/arm
yf1	259	52	1.5	42.46	1024
uf1	260	52	1.5	42.46	1024
vf1	261	52	1.5	42.46	1024
yf2	359	72	1.5	62.94	1536
uf2	360	72	1.5	62.94	1536
vf2	361	72	1.5	62.94	1536
yf3	459	92	9.0	51.46	1024
uf3	460	92	9.0	51.46	1024
vf3	461	92	9.0	51.46	1024
yf4	659	112	1.5	16.86	384
uf4	660	112	1.5	16.86	384
vf4	661	112	1.5	16.86	384
uf5	859	150	2.0	22.48	512
vf5	860	150	2.0	22.48	512
yf5	861	150	2.0	22.48	512
Total channel count:			13,440 up + 13,440 down = 26,880		

The fiber core diameter is chosen to give efficient tracking and good resolution with fibers up to 3 m in length. The photoelectron yield is extrapolated from measurements made at UCLA and Fermilab. Cosmic-ray tests were carried out at UCLA [9] using Kuraray single-clad fibers, of 785 μm core diameter and doped with 1000 ppm of 3HF and 1% PTP, coupled to 3 m of single-clad clear fiber. Cosmic rays passing 60 cm from the optical joint yielded 11.5 photoelectrons, using VLPCs with 80% quantum efficiency. We expect a $> 60\%$ increase in light yield from the multiclad fibers, a 10% increase from the higher dopant level, and up to a 40% loss due to attenuation. (The photon attenuation length in the multiclad scintillating fibers is expected to be 5 m, and in the clear optical fibers, 7.5 m.) Thus a minimum of 12 photons will be incident on the VLPCs for minimum-ionizing tracks passing through the fibers at normal incidence, giving >5 photoelectrons even for VLPCs of 45% quantum efficiency. The staggered doublets should provide RMS position resolution of $\approx$100 μm. With the SDC fiber tracking group we have developed techniques to place fibers to the precision needed to preserve this resolution.

3.5 Particle identification

For complete particle identification, the tracking system just described is augmented with Cherenkov detectors, TRD, calorimetry, and a muon detector. We are exploring possible options for these devices, including the reuse of existing equipment from E789 and other completed experiments.

3.5.1 Ring-imaging Cherenkov counter

Hadron identification is desirable, both to reduce the combinatoric background for decays containing charged kaons and to permit kaon tagging of the second B. These functions could be performed by a series of threshold Cherenkov counters, but a ring-imaging Cherenkov (RICH) counter can identify hadrons over a larger momentum range and with shorter detector length, thereby reducing the total cost of the spectrometer. In addition, a RICH is better able to cope with the high density of particles produced at small angles. Appendix II summarizes the design issues and alternative technologies available for a fast RICH counter. Of the three technologies considered, we propose to choose VLPC readout due to its high speed, high rate capability, high quantum efficiency in the visible, good aging characteristics, and commonality with other systems used in the spectrometer. Working in the visible (rather than the UV as in previous RICH counters) leads to reduced radiator-contamination problems and improved mirror reflectivity.

In detail, the specific choice we have assumed in all simulations for this proposal is a 1.9-m-long radiator of 20% argon and 80% C_4F_{10}. This gives a Cherenkov angle of 50 mr for a $\beta = 1$ particle, and thresholds of 3/10/20 GeV for $\pi/K/p$. An array of 16 mirrors, each 60-cm square and of 1.8-m focal length, will focus the Cherenkov light on two 64-by-64-element hexagonal arrays of Winston cones (on 4-mm centers) at the ring focus above and below the active aperture. Each Winston-cone array will have 4096 clear fibers capturing and transporting the photons to a VLPC array external to the radiator volume. The VLPCs will record $\approx$50 photons per ring at $\beta = 1$ (spread over $\approx$125 cells), determining the Cherenkov-ring radius to $\approx$0.2 mm RMS. This will allow π/K separation to about 100 GeV/c.

3.5.2 Transition-radiation detector

Electron identification using longitudinally-segmented calorimetry typically can reject hadrons at the 10^{-3} level. With the proposed use of single leptons as beauty flavor tags, more stringent rejection is desirable. This can be achieved using the transition radiation emitted by fast (typical $\gamma > 10^4$) electrons. The high proposed interaction rate places stringent requirements on the speed of signal generation. A design for a fast transition-radiation detector (TRD) has been developed and tested at CERN [59]. It employs small (4-mm diameter) thin-walled straw-tubes embedded in a polyethylene-foam radiator. Hadron rejection at the $10^{-2} - 10^{-3}$ level has been demonstrated [59]. The straw tubes have a maximum drift time of 32 ns, somewhat longer than is desirable given the 19-ns bunch spacing of the extracted

beam. However, the TRD will be used to confirm the electron identity of a track which has already been reconstructed using the good timing of the scintillating fibers, thus some pile-up from neighboring buckets is acceptable. We estimate that ≈20k channels will be required.

3.5.3 Calorimetry

An electromagnetic calorimeter is needed for electron identification and photon and π^0 reconstruction. A hadronic calorimeter is desirable to catch electromagnetic shower leakage, help identify muons, and provide a fast trigger which can be used to enhance the beauty fraction of triggered events. It is also possible that a fraction of decays including final-state neutrons and K_L^0's might be reconstructed; E687 has demonstrated this capability using photoproduction, but it remains to be demonstrated in the (dirtier) hadroproduction environment. As shown in Figure 3.4, we propose separate-function electromagnetic and hadronic calorimeters. We next outline our concepts for the electromagnetic calorimeter.

We require the electromagnetic calorimeter to identify electrons and photons, and to measure their energies and positions. Because of the high interaction rate, we are constrained by the occupancy per cell and the total particle flux passing through the calorimeter. Furthermore, to keep the size of the detector elements downstream of the calorimeter within reason, we wish to place the calorimeter as far upstream as possible. As shown in Figure 3.4, we propose to locate the calorimeter 10 m downstream of the target, with a cross-section of 4 m × 3 m. The innermost cells will be located 8 cm from the beam axis. With an anticipated 4 photons per unit rapidity per interaction, at 1 interaction/event there will be 0.07 photons per cell of 10-cm^2 area at this radius. However, the true occupancy is complicated by the lateral size of the showers; this leads us to a design which minimizes the Moliere radius. Furthermore, fluctuations in instantaneous intensity introduce a trigger bias which favors high-multiplicity buckets; thus we are designing for an average intensity of two interactions/event.

Our design choice is a Pb/scintillating-tile calorimeter with fiber readout, as is presently being prototyped for the SDC detector. With sandwiches of 3-mm Pb and 6-mm scintillator, a stochastic term of 10% in the energy resolution is predicted by an EGS4 simulation of the calorimeter. (A similar result was obtained by the SDC collaboration and is shown in Figure 6-6 of the SDC Technical Design Report.) The constant term should be kept at or below 2% for this device. Twenty-seven radiation lengths are sufficient for 95% containment of showers up to 200 GeV. Experimental studies of a device of similar design have shown that over 80% of the shower is contained within a cone of radius 3.2 cm about the shower axis [60], thus we believe segmentation at this level is feasible. Since the occupancy falls off quadratically with radius, we use cells of 3.2 cm by 3.2 cm from 8 to 40 cm from the beam, 6.4 cm by 6.4 cm from 40 to 78.4 cm, and 12.8 cm by 12.8 cm beyond 78.4 cm. The total number of towers is then 1,420. With two segments in depth, 2,840 readout channels are required.

The issue of possible radiation damage can be addressed by considering the particle flux at shower maximum. For a 20-GeV shower, we expect 200 minimum-ionizing particles (mip) at shower maximum [61]. In the worst case this will be totally contained within one tower of area 10 cm^2. Since the shower occupancy is 0.07/interaction, we have 1.4 mip per cm^2 per interaction. For a run of 1.5×10^{14} interactions the cumulative dose will be 7 MRad. The measurements of Bross and Pla-Dalmau [54] on 3HF-doped polystyrene indicate that rapid exposure to 10 MRad can reduce light yield by about 20%. For concentrations of 1% 3HF and above, annealing by exposure to air at room temperature for about 3 weeks restores the light yield to 97% of the unexposed value. Thus we do not expect severe radiation damage under our conditions, but will monitor the scintillator response throughout the run. The mechanical design will allow for replacement of the innermost towers if needed. This choice of scintillator leads us to choose phototubes with multialkali cathodes to match the emission spectrum of the 3HF fluor.

While the energy sharing among the calorimeter towers will give some spatial information, we are exploring the construction of a preshower sampler or a shower-maximum position detector. The former can enhance the π/e rejection and provide precise position measurement for photons; the latter can also give precise position information and might improve the two-shower resolution. We would employ a design based on scintillating strips read out by fibers and VLPCs. With 2-mm strips, a total of 4,500 channels in either detector would provide y-u-v small-angle stereo.

Due to the larger transverse spread of hadron showers, the hadron calorimeter need not be as finely segmented as the electromagnetic. We propose an Fe/scintillator tower array, of transverse segmentation one-half that of the electromagnetic calorimeter, and with only one segment in depth. The total channel count is thus 360.

For the calorimeters themselves the per-channel cost includes \$100 for towers, \$100 for phototubes, and \$50 for ADCs and cabling. (We anticipate the need for 12-bit dynamic range; by contrast, the 16-bit KTeV ADCs are estimated to cost \$170/channel.) The total calorimeter cost is thus $\approx$\$1M. An alternative design which reduces the occupancy per tower close to the beam uses tungsten as a converter and is also under study.

3.5.4 Muon identification

With some modification, the existing E789 muon detector is suitable for use in the proposed experiment. It consists of scintillation hodoscopes and proportional-tube chambers covering a $3 \times 3\,m^2$ area, interspersed with zinc and concrete absorber, and provides position measurement in x and y with 4-mm resolution. The detectors and absorbers will be rearranged to create a 10 cm gap at beam height and to provide small-angle stereo measurement.

3.6 Triggering

The goal of the triggering system is to reduce the event rate from the 53 MHz accelerator RF frequency to the 5 – 25 kHz which can be written to tape. The least biased trigger approach

is one based on secondary-vertex detection, and we propose to trigger on vertices at Level 1 using the Cherenkov-based optical impact-parameter trigger already under development by our collaboration [1,2]. In addition, Level-1 triggers selecting high-E_t events and events containing high-p_t leptons or photons can be provided by the calorimeters and the muon system; we intend to employ these as redundant alternatives to the optical trigger which can be used to study its efficiency. Subsequent levels of trigger can make use of track information from the silicon-strip and scintillating-fiber planes in fast matrix, memory-lookup, or neural-network systems, and the final trigger decision can be made by a fast processor system, to select events containing tracks consistent with moderate- or high-mass states decaying downstream of the target. All of these approaches are under investigation, and we intend to present detailed simulation results shortly.

3.6.1 Level-1 (main): optical impact-parameter trigger

The optical trigger, conceived by Charpak, Giomataris, and Lederman [1], is a powerful technological advance in triggering on displaced vertices. It consists of a thin spherical shell of transparent crystal of refractive index n_1, focussed on the (point-like) target and surrounded by a medium of refractive index n_2 (see Figure 3.6). The indices are chosen so that

$$n_1^2 - n_2^2 = 1 - \epsilon,$$

with ϵ small and positive. It is straightforward to show that under this condition, Cherenkov light emitted within the crystal by particles originating in the target escapes through the convex face of the crystal; in contrast, particles whose tracks have sufficiently large impact parameter at the target emit Cherenkov light a portion of which is trapped within the crystal by total internal reflection. Trapped Cherenkov photons emerging at the edge of the radiator are imaged by an array of clear multiclad optical fibers. The acceptance angle of the fibers is $\pm 30°$ and their photon attenuation length is 9 m. The fibers transmit the photons to VLPCs, which are located 3 m from the beam axis.

Appendix III discusses optical-trigger design issues in detail. Our current design is a 4-shell sandwich of sapphire radiators clad with quartz or liquid-CCl_4. The total thickness is 2.5% of a radiation length (we have verified by Monte Carlo simulation that this makes only a small contribution to the mass resolution at the D and a negligible contribution at the B). With CCl_4 cladding we calculate 2.5 photoelectrons detected per charged particle at an impact parameter of $500\,\mu$m. Simulations based on PYTHIA indicate that requiring at least 2 photoelectrons detected should then provide a rejection of 10 against minimum-bias events, with beauty and charm efficiencies of 70% and 30% (respectively). We are working on approaches for achieving additional minimum-bias rejection based on simple pattern-recognition using the detected image; a fallback position which is capable of ≈ 100 rejection is to divide the radiator into azimuthal segments and require a two-fold coincidence [62]. The design will continue to evolve in concert with the ongoing test-beam effort at CERN. This effort will address such issues as the optimal choice of radiator and cladding materi-

als, optimization of the optics for light-collection efficiency and chromatic aberration, and detailed studies of backgrounds and methods for their rejection.

First tests of the optical-trigger principle have been carried out using test beam at Fermilab and at CERN. The results are encouraging and have been submitted for publication [2, 3] (see Appendix IV). The performance of a realistic trigger, including VLPC readout, will be tested this summer in a test beam at the CERN PS.

3.6.2 Level-1 (alternate): E_t trigger

Based on the differential cross section vs. E_t measured in 800-GeV p-Pb interactions by E557/672 [63, 64], Figure 3.7 shows the efficiency for minimum-bias events vs. E_t threshold. (We have not yet included in this calculation effects due to calorimeter resolution or magnetic deflection of charged particles.) One sees that (for example) an 8-GeV E_t threshold gives a rejection factor of 4, and a 10.5-GeV threshold 10.

To evaluate the efficacy of an E_t trigger for charm or beauty, one needs to model the E_t distribution of heavy-quark events produced in a heavy target. A commonly used model, that of the PYTHIA Monte Carlo, is unsuitable in that it lacks nuclear effects; PYTHIA predicts $< E_t >= 1.6\,\mathrm{GeV}$ for minimum-bias events, in disagreement with the heavy-target data [64]. PYTHIA's predicted 8-GeV mean E_t for beauty events is thus suspect in the case of a heavy target. The FRITIOF Monte Carlo does model nuclear effects but does not contain a $b\bar{b}$ generator. To estimate beauty efficiency vs. E_t threshold then requires a procedure such as coupling PYTHIA $b\bar{b}$ generation with FRITIOF nuclear fragmentation effects. This study is in progress.

A simple preliminary estimate suggests that an E_t trigger for beauty may be effective: if the 8-GeV mean E_t predicted by PYTHIA for beauty adds linearly to the 6-GeV mean E_t observed by E557/672 [64] for minimum-bias events, an 8-GeV threshold in E_t could have efficiency close to 1. These effects are rather subtle, and their Monte-Carlo simulation is unlikely to be sufficiently trustworthy to depend on in designing a beauty trigger. We therefore intend to study the efficacy of an E_t trigger for beauty experimentally as part of the proposed experiment.

3.6.3 Level-1 (alternate): lepton/photon triggers

A coarse muon coincidence will be generated using sixteen-channel summed signals from the y detectors in the two muon planes. Likewise a series of fast calorimeter outputs will be generated for sections of the electromagnetic calorimeter. Using standard NIM logic a $(\mathrm{lepton} \oplus \mathrm{photon})_{\mathrm{UP}} \cdot (\mathrm{lepton} \oplus \mathrm{photon})_{\mathrm{DOWN}}$ signal can be formed which will be used as an alternate Level-1 trigger. Single-lepton and -photon triggers will also be provided, with p_t thresholds adjusted so as to give acceptable trigger rates. These alternate triggers are invaluable in maximizing the sensitivity to heavy-quark decays which include leptons or photons. The lepton triggers complement the E_t trigger in that heavy-quark events with low calorimetric E_t typically contain final-state muons.

3.6.4 Level-2: silicon trigger matrices

A fast triple coincidence of neighbouring silicon planes can be used to trigger on tracks with an apparent finite impact parameter. The geometrical spacing of the silicon planes is arranged so that neighbouring y planes are at distances of z, $1.17z$, and $1.38z$. Thus, the projection of single 50-μm-wide microstrips from the first and last planes to the target defines an impact parameter with an RMS resolution of about 100 μm. The triple coincidence with the middle plane serves to suppress chance coincidences from neighbouring tracks in the silicon. The matrix can be set to trigger on impact parameters from 100 to 1000 μm. Simulations show that this gives an efficiency of almost 100% for B decays that fire the Level-1 optical trigger, and a further rejection of at least ten against the events that fool the optical trigger: delta rays, low-energy backgrounds, etc.

The matrix required is the classic almost-diagonal matrix that can be implemented in fast gate-array logic, possibly arranged in a neural net to facilitate tuning for the needed rejection. A coincidence between a matrix output in the upper silicon planes and the lower silicon planes constitutes the second-level trigger. Since the average track passes through six y silicon planes, the inefficiencies of this trigger due to single missing silicon hits should be very low. Detailed simulations of this trigger strategy are in progress.

3.6.5 Level-3: trigger processor

E789 demonstrated the efficacy of a trackfinding trigger processor in reconstructing charm decay vertices on-line. The processor [7] was constructed from Nevis Laboratories processor modules [65] and used hits in the bend-view drift chambers, hodoscopes, calorimeter, muon detectors, and silicon detectors to find tracks in two dimensions, requiring the presence of tracks consistent with a decay vertex downstream of the target. (For monitoring purposes, a prescaled sample of events failing the processor requirements was also recorded.) The processor provided a rejection factor of 10 for noncharm events. Due to its relatively simple algorithm, it was rather sensitive to inefficiencies in the silicon planes, leading to an efficiency for $D \rightarrow$ dihadron events of 50% and hence an overall enhancement factor of 5.

A more complex algorithm has been implemented in a Nevis processor by the E690 collaboration and successfully used to carry out the E690 first-pass data reduction, reconstructing 5.4×10^9 events in $\approx$5 weeks of processing time [66]. While the suitability of the Nevis approach for implementing complex pattern-recognition algorithms has thus been amply demonstrated, the early-1980s technology (ECL-10,000 MSI integrated circuits) which it represents has been superseded by recent developments. Using field-programmable gate arrays, application-specific integrated circuits, or full-custom integrated circuits, it is now possible to construct modules based on the Nevis approach but featuring significantly improved speed, density, reliability, and ease of use [67]. We thus propose to update the processor implementation using whichever combination of these technologies proves most cost-effective.

3.7 Data acquisition

3.7.1 Front end

Fully-pipelined front-end electronics are under development for KTeV and SSC experiments. We anticipate that a similar system is appropriate for the proposed experiment. The preamplifiers of the silicon, scintillating-fiber, and RICH detectors will put out parallel streams of pulses which can be discriminated and stored 1 bit/channel in digital pipelines. Since the first- and second-level triggers are quite fast, a pipeline depth of some tens of buckets should suffice. When the first- and second-level triggers are satisfied, the appropriate pipeline bucket needs to be retrieved, sparsified, and read into event buffers in $\sim 1\,\mu$s for processing by the trigger processor.

The Fermilab QPA02 ASIC preamplifier used in E771 and E789 is suitable for readout of the silicon and fiber systems. However, a new scheme for mounting the preamplifier chips on the silicon detectors is desirable, to reduce both the capacitance of the fanout traces and the tendency of the QPA02 to oscillate. The discriminator could be based on the Berkeley design used in E789 or the Fermilab design used in E771. In addition to feeding the pipelines, the discriminator needs to provide prompt outputs for the trigger matrices. The digital pipeline need not be as sophisticated as that being designed for KTeV, since for our purpose it should handle streams of independent bits rather than 16-bit words on which arithmetic is to be performed. We believe that a simple pipeline chip suitable for our experiment would be a natural building block for the more sophisticated KTeV application. For the calorimeters, the 16-bit KTeV/SSC phototube-base/ADC could be employed, but we believe that our (less demanding) application does not justify the cost. We propose to use instead a conventional phototube base with delay cable and remote 12-bit ADC.

3.7.2 Back end

The cost of computing continues to fall by about a factor of 2 per year. In 1991-92 E789 recorded $> 10^9$ events, which will all have been reconstructed during the $\approx$1-year period ending in the summer of 1993. While E791 arguably recorded more data than is optimal to process at this time (2×10^{10} events), it appears likely that by 1997 it may be practical to analyze $\sim 10^{11}$ events/year (see Figure 3.8). The physics goals presented above will require the amassing of high statistics for charm decays. In view of the difficulty of achieving adequate efficiency for charm with better than 10^{-3} trigger rejection, we believe it is appropriate to plan for $\sim 10^{11}$ events recorded per run. If the trigger functions well, we may find we do not need this full capacity, however it would be unwise to plan on significantly lower bandwidth.

The above bandwidth is a straightforward extrapolation of what has been achieved by E690 and E791, and we believe it is within the scope of the DART data-acquisition system under development by the Fermilab Computing Division. We expect our events to be similar in length to those of E791 ($\approx$10 kb). Since the construction of the E791 data-recording system, which employs 40 8-mm Exabyte tape drives in parallel, Exabyte has developed

improved drives which provide a factor 2.5 in density and a factor 2 in data rate. Considering that the E791 data set was recorded only during the latter half of the run, one sees that a $\sim 10^{11}$-event/run recording capability already exists. Another alternative is the Honeywell VLDS drives employed by E690; a single VLDS drive allowed the recording of 5.4×10^9 events during the few-week E690 run.

3.8 Beam and target

The optical impact-parameter trigger requires a small interaction region. To achieve this we intend to focus a primary proton beam on a high-Z (probably gold) target approximately $300\,\mu$m in diameter $\times$ 2 mm in thickness. Depending on the target chosen and the limiting rates in the spectrometer, beam intensities up to about 10^{11} protons per pulse may be required.

The target will be mounted by thin filaments to a remotely-controlled stage, which can be translated in all three dimensions to permit precise alignment relative to the optical trigger. As in E789, the target should be located in vacuum to eliminate possible confusion between decay vertices and downstream interactions. The thin beam-vacuum window will be located just downstream of the optical trigger and just upstream of the silicon-detector box. Downstream of the silicon detectors, the beam will be transported through the spectrometer to the dump via a thin-walled vacuum pipe.

It is not yet clear in what beam line the proposed experiment could best be carried out. One option is Meson East, with the apparatus to be installed upstream of the large "SM12" analyzing magnet and beam dump. E789 targeted $\approx 70\%$ of the Meson-East beam on the thin edge of a gold target $250\,\mu$m high $\times$ 5 cm wide $\times$ 3 mm thick, at intensities up to 6×10^{10} protons per pulse. To achieve a comparable targeting fraction on a 300-μm-diameter target will require some rearrangement of the existing focussing elements in the beam line. The optimal way to implement this is under study.

In the Meson-East option, some of the new equipment could be installed for testing before the 1994/95 run and debugged using beam halo during the short E866 run. (The silicon detectors could be in the tunnel during this period but could not be moved into their final positions until the completion of E866.) Upon completion of E866, the new target and the optical trigger would be installed. We are also investigating the suitability of other Fermilab beam lines which may become available.

4 BACKGROUNDS

In an experiment such as proposed here, in which small signals are sought, backgrounds are a prime concern. Some of us [68] have done extensive studies in the past on backgrounds to the observation of beauty decays in fixed-target hadroproduction, and we believe that these studies remain applicable to the proposed experiment. E789 has demonstrated the power of vertex cuts, in a geometry comparable to the one proposed, to suppress adequately light-quark backgrounds to charm and beauty (see Figure 4.1) [69]. One must then consider whether backgrounds from the heavy-quark events themselves will compromise the proposed measurements, as well as whether differences between the proposed experiment and E789 affect the light-quark background in detail.

4.1 Dihadronic beauty decays

Due to their small expected banching ratios and the small number of constraints in a two-prong vertex fit, dihadronic beauty decays pose an especially challenging background problem. Events from the QCD dihadron continuum will occasionally fake decays downstream of the target due to large scatters in the first silicon plane or pattern-recognition confusion in the vertex reconstruction. In modes containing kaons or protons, Cherenkov hadron identification provides a suppression factor ranging from 3 to over 10 against continuum events. In E789, superb mass resolution, combined with vertex cuts, was key to reducing the QCD $\pi\pi$ continuum to the $< 10^{-5}$ beauty-branching-ratio level. It is not as easy to achieve $\approx$0.2% mass resolution for $B^0 \rightarrow$ dihadrons in a large-acceptance experiment such as proposed here; Monte-Carlo simulation of the proposed apparatus indicates 0.5% RMS mass resolution for $B^0 \rightarrow \pi^+\pi^-$ (see Appendix I). This mass resolution will be adequate in view of the factor $\approx$100 rejection against light-quark events which the optical trigger will provide (note that the optical trigger is insensitive to scattering in the silicon and to tracking pattern-recognition problems).

Another concern is beauty decays in which there are missing neutrals, for example $B^0 \rightarrow \rho^+\pi^-$ followed by $\rho^+ \rightarrow \pi^+\pi^0$. In the Wirbel-Stech-Bauer model [24] the branching ratio for this mode is predicted to be $\approx$3 times that for $B^0 \rightarrow \pi^+\pi^-$. However, the mass resolution of the proposed spectrometer is sufficient to leave only a negligible fraction of such decays in the $B^0 \rightarrow \pi^+\pi^-$ mass region (see Figure 4.2).

4.2 $b \rightarrow s\gamma$

We expect that the dominant background to the search for $b \rightarrow s\gamma$ will be other photons (primarily from π^0 decay) in the beauty event. Appendix I details the simulations in progress to study this background and its rejection. Preliminary results are promising, indicating that a rejection factor $> 10^3$ can be achieved while retaining signal efficiency $> 10\%$.

4.3 Other modes

Simulations of backgrounds to other modes of interest are also in progress, but results at this time are too preliminary to report.

5 COMPETITION

Studies of B physics at CESR, DORIS, and LEP, and at $\bar{p}p$ colliders such as S$\bar{p}p$S and the Tevatron, show that much B physics will be carried out at existing e^+e^- and $\bar{p}p$ colliders. However, particular goals of this proposal, such as the study of $B \rightarrow X + \gamma$ and B_s mixing, will be very difficult at both e^+e^- and $\bar{p}p$ colliders. At the e^+e^- colliders the total sample of $b\bar{b}$ final states is limited, in the case of LEP to $\sim 10^6$ produced events in the final data set, and in the case of CLEO to $\sim 10^7$ produced events by 1996. For $\bar{p}p$ colliders the rate of $b\bar{b}$ production is much greater, but a restrictive trigger is required to reduce the rate to an acceptable level, and in existing detectors the tagging efficiency for the other B in the event is quite small. We therefore believe that a dedicated optically-triggered fixed-target experiment is competitive with these experiments. We note that charm studies are even more difficult at the e^+e^- and $\bar{p}p$ machines, since the experimental signature of high-$p_\perp$ leptons used for $b\bar{b}$ tagging and triggering is less effective for charm. Even an e^+e^- τ-charm factory would not provide an adequate rate to search for D^0 mixing at the level suggested in this proposal.

6 COST ESTIMATES

The preliminary estimated breakdown of costs is as follows:

1) Silicon Detectors

Silicon (30 double-sided wafers + spares)	\$300k
Mounts	50k
Preamps (20k channels)	100k
Discriminators/Delay/Latch (20k channels)	500k
A/C & RF shielding	50k
Total	\$1.0M

2) Scintillating-Fiber Tracking

Rockwell International Science Center has prepared a cost estimate for the SSC Fiber Tracking group giving a per-channel cost of \$52, broken down as follows:

Fibers and mechanical support	\$ 2
VLPCs and cryogenic cassettes:	25
Amplifiers:	5
Readout electronics, cables, & connectors:	20

giving the following total cost:

27k channels $\times$ \$52/channel = \$1.4M

3) RICH

VLPC readout (8k channels)	\$400k
Tank, mirrors, gas system	500k
Total	\$0.9M

4) TRD \$1.0M

5) Calorimeters

Electromagnetic calorimeter:	
Towers	\$300k
Phototubes	300k

ADCs & cabling	150k	
Preshower or shower-maximum detector:	200k	
Hadron calorimeter:		
Towers	40k	
Phototubes	40k	
ADCs & cabling	20k	
Total		\$1.1M
6) Trigger and DAQ system		\$1.0M
Grand Total		\$6.4M

7 PROPOSED SCHEDULE

7.1 Near-term schedule

- Run 1 (1994/95) Test as much as possible: at least a portion of the silicon and fibers and the optical trigger, a partial RICH counter, and an E_t trigger using a borrowed calorimeter

- Run 2 (1996/97) Full run with full coverage, triggering, and particle-ID

7.2 Longer-term prospects

Experience teaches that in high-rate experiments aiming to detect small signals, each new order-of-magnitude in sensitivity brings with it new problems, the nature of which is often difficult to anticipate in advance. (For example, E70/288/494, before discovering the b quark, took data in Proton Center for five years; this experience was crucial and provided ultimately a factor > 1000 in sensitivity.) We intend to carry out a program of staged upgrades, proceeding in a natural way towards a CP-level experiment by the end of the decade.

Three ideas for achieving CP-level sensitivity have been considered. One of us [4] has sketched an experiment based on radiation-hard silicon pixel detectors which appears to have the necessary interaction-rate capability. Pixel detectors are under intensive development by several groups [47] in preparation for experiments at LHC and SSC, and it is likely that they will become available in radiation-hard versions before the end of the decade.

The second idea [5] is to take advantage of the strong energy dependence of the beauty cross section [70], yet retain the relative ease of triggering and secondary-vertex reconstruction provided by fixed-target geometry, by arranging collisions between proton beams of widely differing energies. This might be achieved by modification of the Main Injector to allow collisions between its beam and that of the Tevatron; to preserve the desired small interaction region, the beams should be made to cross at a modest angle. Preliminary discussions with Main Injector accelerator physicists indicate that such a scheme may be feasible [71]. More generally, the detector might be moved to a higher-energy interaction region, for example fixed-target or collider operation at LHC or SSC. Even internal-target operation at the SSC HEB would provide an order-of-magnitude increase in cross section compared to 800 GeV, probably sufficient for sensitive CP-violation measurements. We note that the proposed detector bears a generic resemblance to forward spectrometers proposed for Tevatron- and SSC-collider operation and could straightforwardly be augmented at large angles to improve the beauty acceptance at $2 - 40$ TeV.

A third possibility is that a spectrometer composed largely of silicon microstrip detectors might be operable beyond the generally accepted limit of irradiation, either through improvements in silicon-detector fabrication techniques or through explicit engineering of the mounting system for ease of chip replacement, so that damaged detectors might be replaced

several times in the course of a run. (The latter approach has been proposed by the ARGUS group for an internal-target B-decay CP-violation experiment at HERA [10].)

We recognize that any or all of these techniques may prove insufficient to reach CP sensitivity. However, even in that case, one will have done substantial beauty and charm production and decay physics, made precise mass and lifetime measurements, and developed techniques for triggering, vertex reconstruction, B tagging, and particle detection and identification at high rates. (It would help to understand some of these technical issues before building SSC and LHC beauty experiments!)

APPENDIX I: DETAILS OF SIMULATION STUDIES

We are carrying out several simulation studies for this proposal. They range from simple aperture-based estimates of geometrical acceptance to full GEANT simulation of the proposed apparatus, using PYTHIA and FRITIOF event generators.

I.1 Acceptance simulation

To estimate the geometrical acceptance of the proposed spectrometer, we generate individual charm or beauty particles according to phenomenological models and force them to decay in particular modes of interest. We then track the decay products through a simulation of the apparatus which includes Moliere scattering in all detector materials. Production models used are listed in Table I.1. Due to the large angular coverage of the proposed spectrometer, the acceptance is relatively insensitive to the details of the production and decay dynamics and depends to first order only on the number of particles in the final state. This is summarized in Table I.2. Acceptance per prong averages somewhat lower for charm than for beauty; we attribute this to the lower average laboratory-frame momentum of charm decay products, which increases the probability of a particle being deflected out of the aperture by the analyzing magnet. Figure I.1 shows the daughter momentum spectra and the x_F and p_t distributions of charm and beauty particles for which all decay products are accepted.

TABLE I.1 Production models used in acceptance simulations

model	quark	$dN/d(p_t)^2$	dN/dx_F
1	charm	$\exp(-p_t^2/2)$	$(1-\|x_F\|)^{7.5}$
2	charm	$\exp(-p_t^2/2.275)$	$\exp(-40x_F^2)$
3	beauty	$\exp(-p_t^2/5.275)$	$\exp(-18x_F^2)$
4	beauty	$\exp(-p_t^4/125)$	$\exp(-18x_F^2)$
5	beauty	PYTHIA	PYTHIA

TABLE I.2 Geometrical acceptance for various decays modes and models

model	mode	acceptance	RMS mass resolution (MeV)
1	$D^0 \to K^-\pi^+$	0.45 ± 0.02	6.7 ± 0.3
2	$D^0 \to K^-\pi^+$	0.47 ± 0.01	6.5
3	$B^0 \to \pi^+\pi^-$	0.55 ± 0.01	23.5 ± 0.8
4	$B^0 \to \pi^+\pi^-$	0.55 ± 0.02	25 ± 1
4	$B^\pm \to J/\psi K^\pm$	0.42 ± 0.02*	19 ± 1
4	$B^0 \to J/\psi K_s$	0.16 ± 0.01*	17 ± 2
4	$B^0 \to \bar{D}^0\rho^0 \to K^+\pi^-\pi^+\pi^-$	0.29 ± 0.02	28 ± 2

* assuming K_s is reconstructed in the silicon detectors; acceptance doubles if K_s allowed to decay inside analyzing magnet

I.2 Resolution simulation

To study resolution effects, we add least-squares trackfitting to the simulation just described. We have also used a more detailed GEANT-based simulation, featuring Kalman-filter trackfitting, to verify the results of the first simulation. A magnet with 0.5-GeV p_t kick is assumed, with the detector dimensions, locations, and pitches as given in Section 3 above. Figure I.2 shows the reconstructed mass distribution for $B^0 \to \pi^+\pi^-$ decays. Figure I.3 shows the resolution in decay distance ($z_{\text{reconstructed}} - z_{\text{thrown}}$) and in proper time ($\tau_{\text{reconstructed}} - \tau_{\text{thrown}}$). The RMS mass resolution for various modes is summarized in Table I.2.

I.3 Pattern-recognition simulation

A key issue is the performance of the proposed detector configuration for pattern recognition. Sufficient redundancy is required for reliable trackfinding with good rejection against ghost tracks; on the other hand, too many redundant measurements not only wastes resources but degrades resolution by increasing multiple scattering. The proposed geometrically-spaced silicon detectors provide 12 hits per track on average, independent of angle from 8 to 150 mr. A full simulation of track reconstruction is quite involved, and while we have begun such a study, we do not yet have results to present.

I.4 $b \to s\gamma$ simulation

Simulation studies are being conducted of the photons from the inclusive decay $b \to s\gamma$ and the exclusive decay $B \to K^{*0}\gamma$ using the Monte Carlo program PYTHIA to generate B events. Since $b \to s\gamma$ decays are not implemented in PYTHIA, we treat the decay as two-body, assuming that the s and spectator quarks hadronise into a state with a mean mass halfway between the K^* and the K_4^*. This generates a mass distribution with FWHM

equal to the K_4^* - K^* mass difference. The shape is a gaussian, truncated at the low end at the mass of the K^* and at the high end at the mass of the B.

We assume an energy resolution of $\frac{10\%}{\sqrt{E}}$, an angular resolution of 1 mr for γ's, and (since the calorimetric photon measurement will dominate the resolution) a perfect momentum resolution for hadrons.

The transverse momentum distributions for γ's from B events have been obtained. The B background includes all γ's; the signal includes only those γ's originating from the b quark. The p_t spectrum of γ's from non-B events is also obtained to permit background subtraction.

According to Ali the Standard-Model prediction for the branching ratio of $b \rightarrow s\gamma$ is $(2 \sim 5) \times 10^{-4}$. Assuming a branching ratio of 4×10^{-4}, 20 signal events correspond to the 50,000 background events we generated. Since even at the peak of the signal p_t spectrum the background exceeds the signal by 2 orders of magnitude, we have investigated several cuts to see whether we can extract the signal from the background.

In order to suppress γ's from π^0, we exclude from the analysis all γ's which are consistent (within the calorimeter resolution) with making up a π^0 in combination with any other γ in the event. Various $\gamma\gamma$ mass-range cuts are examined. Excluding the range $0 < m_{\gamma\gamma} < 0.2\,\mathrm{GeV}$, the signal-to-background ratio is improved by a factor of 140 with a signal retention of 55%.

At the high end of the p_t spectrum the signal-to-background ratio is further increased by a cut on the energy of the gammas. The E_γ distribution from background events drops off at 40 GeV, whereas the distribution for signal events is relatively uniform from 0 to 120 GeV. Requiring $E_\gamma > 40\,\mathrm{GeV}$, the signal-to-background ratio is improved by an overall factor of 2500, with a background retention of 15%. This cut is so effective that we are left with too few simulated background events to complete the analysis, and much higher Monte-Carlo statistics are needed.

Preliminary studies are also being conducted of the exclusive decay mode $B \rightarrow K^{*0}\gamma$. The π^0 mass-range cut used above to veto γ's from π^0 is again applied. The next cut used is to require $K\pi$ pairs to fall within the K^* peak by vetoing events in which the invariant mass is outside the range 0.7 to 1.1 GeV. Following this the $K^*\gamma$ pairs are required to lie near the B mass, from 5.0 to 5.5 Gev. The final cut is to veto events in which the opening angle of the $K^*\gamma$ pairs is outside the range 24 to 560 mr. Again these cuts are so effective that we need to continue the study with higher statistics. The results are promising, and we believe that with optimised cuts we may be able to distinguish the signal from the background.

APPENDIX II: RICH DESIGN ISSUES

The RICH is to provide π/K discrimination up to $\approx$100 GeV/c with a kaon threshold of $\approx$10 GeV. It is desired to cover the entire angular range of the proposed spectrometer (8 to 150 mr in y and $\pm$200 mr in x) with a detector of minimal length and cost. The central region must allow for the passage of the beam protons. There is still much design work to be done, but this section will provide a guide for what is needed and rough cost estimates. For a first run, one might very well use a RICH from another experiment, with some upgrades to make it usable at our interaction rates.

Several current research projects are attempting to design RICH detectors similar to what would be required for this experiment [72]. Demanding applications such as LHC and SSC experiments illustrate the range of approaches which appear feasible at this time. Detailed studies for our proposed geometry are in progress; we describe here our current understanding, which is somewhat preliminary.

II.1 RICH mechanics and optics

Table II.1 summarizes the relevant parameters of three gases covering the range in kaon threshold which may be of interest:

TABLE II.1 Properties of typical radiator gases

gas	n^*	$\pi/K/p$ threshold (GeV/c)	photons/m (eV^{-1})	p@1/0.5 mr sep. (GeV/c)	$\theta_C@\beta=1$ (mr)
C_4F_{10}	1.00153	2.5/8.9/17	110	45/65	55.2
Xe	1.000705	3.7/13/25	50	55/78	37.5
Ar	1.000283	5.9/21/39	20	70/98	24.0

* C_4F_{10} at 177 nm, Xe and Ar for D light, n for Ar increases to 1.000379 at 150 nm.

Previous RICH detectors have typically achieved 1 mr resolution. A detailed analysis should include the improvement in performance arising from multiple detected photons per ring, but the momenta given in Table II.1 at which π and K are separated by 1 and 0.5 mr are indicative of the approximate performance limits expected for a given set of thresholds. At the limit, resolution will be dominated by optical defects of the mirrors for a short RICH. Mirrors produced by slumping methods have been made with $\approx$1 mr dispersion, so such mirrors may be suitable. Slumped mirrors, which are typically thinner than the ground mirrors used e.g. in the E605 RICH, may be desirable to reduce scattering, photon conversions, etc.

We now consider the physical constraints on the size of the RICH in order to have an idea of the size and type of photon detectors that will be needed. The goal is to keep the RICH as short as possible in order to reduce the cost of the downstream components of the

spectrometer. A quick calculation shows that if one uses a spherical mirror to focus light on detectors as in E605/789 there is a problem with a short radiator: in order for the light rays to miss the front surface of the radiator, the mirror must be at a fairly large angle. This leads to problems with astigmatism (see e.g. Jenkins and White [73]).

The calculation given here assumes the front face of the RICH is at $z = 3.8\,\mathrm{m}$, thus 150 mr coverage corresponds to a height of $\pm 0.57\,\mathrm{m}$; we assume a front surface of size $\pm 0.70\,\mathrm{m}$ to allow for the frames necessary to mount the photon detector apparatus. The inclination angle of the mirrors relative to the beam axis depends on the radiator depth and the mirror size. Table II.2 gives the minimum mirror angle for particles striking the mirror array.

TABLE II.2 Configurations considered for aberration analysis

case	mirror size (cm)	radiator thickness (m)	minimum mirror angle	# mirrors
1	25.40	1	16.0°	6 x 6
2	40.64	1	13.9°	4 x 4
3	25.40	2	8.0°	8 x 8
4	33.02	2	7.6°	6 x 6
5	48.26	2	6.5°	4 x 4

Using equations from Klein [74], one finds for a spherical mirror that the off-axis aberration is

$$W = -[\frac{r^4}{32f^3} + \frac{r^3}{4f^2}\tan\beta\cos\phi + r\tan^3\beta\cos\phi + \frac{r^2}{4f}\tan^2\beta\,(2\cos^2\phi + 1)]\,,$$

the lateral spherical aberration from a circular zone of radius r is

$$x = -\frac{r^3}{8f^2}\,,$$

the comatic circle will have a radius

$$A = \frac{r^2}{4f}\tan\beta\,,$$

and the compromising best focus for astigmatism will give a circle of radius

$$\delta = \frac{1}{2}r\tan^2\beta\,,$$

where β is the angle of the track relative to the optical axis of the mirror, which varies from the minimum mirror angle to the minimum mirror angle plus the angle subtended by the mirror. The radius r would normally be the radius of the mirror, but since only a cone of

radius $L \tan\theta_C$ is illuminated, where L is the radiator length and θ_C is the Cherenkov angle, we should use $L \tan\theta_C$ instead of r in calculating the above aberrations. The focal length f is assumed to be roughly the length of the radiator. Since astigmatism is the major problem here, increasing the focal length will not help, e.g. with a mirror of 3 m focal length and a 2-m-long radiator, the minimum mirror angle must be increased. Values for each of the aberrations for the five cases given above are tabulated below assuming C_4F_{10} as the radiator gas. The first value is for the minimum β and the second for the maximum β (note: x does not depend on β).

TABLE II.3 Aberrations for each configuration

case	W (mm)	x (mm)	A (mm)	δ (mm)
1	1.4/2.4	0.2	0.2/0.2	2.2/3.2
2	0.9/2.3	0.2	0.2/0.2	1.6/3.0
3	0.2/0.4	<0.1	<0.1/<0.1	0.5/0.9
4	0.1/0.4	<0.1	<0.1/<0.1	0.5/1.0
5	0.1/0.5	<0.1	<0.1/<0.1	0.3/1.0

Since for a mirrorof 1 m focal length, 1 mr corresponds to 1 mm at the image plane, one can see that astigmatism rules out a 1 m radiator. A 2 m radiator is tolerable.

II.2 RICH photon detector

Per interaction the photon detector needs to cope with ~10 tracks above threshold, each giving ~10 detected photons. At 1 interaction/RF-bucket this is a 5 GHz photon rate. In a run of 10^{14} interactions, a detector based on wire chambers operating at a gas gain of 10^5 would generate ~10^{21} electrons, or 10^{15} electrons/mm^2 for 1 m^2 detector area. (The central regions would see even a higher rate).

These estimates imply that the photon detector will need:

- Pad or pixel readout
- <19 ns time resolution
- High rate capability
- Radiation hardness (good resistance to aging)
- A fast readout system.

We next estimate of the number of pads needed. Assuming a 2 m focal length, 2 mm position resolution gives 1 mr angular resolution. This requires pads approximately 7×7 mm^2.

Case 5 minimizes the channel count, using two detectors each 50 cm wide by 50 cm high: 70×70 pads = 4,900 pads per detector. This assumes each mirror is focussed on a slightly different area of the detector to avoid confusion in reconstruction.

Three photon-detection technologies are under consideration: solid CsI photocathodes coupled to MWPCs, MWPCS operated in a photosensitive gas, and VLPCs.

CsI photodetectors are currently under development at Fermilab and in Europe [75, 76, 77]. Their main drawback is the 30% drop in quantum efficiency observed in aging tests after 2×10^{14} electrons/mm^2 [77]. This is an order of magnitude below the average electron dose we anticipate. If this problem can be overcome, or if the detector does not degrade further at higher dose, this would likely be the ideal detector due to its very good time resolution and compatibility with quartz windows.

A fast TEA-based photon chamber for RICH has been discussed [78] by Lund-Jensen *et al.* It is an MWPC filled with CH_4 bubbled through TEA at 20°C. Monte-Carlo studies give 15 ns time resolution [78]. Aging of a TEA chamber may be a concern, but with proper design, replacing or cleaning bad wires or chambers during the run could be possible. Due to the high ionization potential of TEA, CaF_2 windows are required; we would plan to reuse the E605 RICH windows.

The third idea under consideration is an array of VLPC detectors coupled by clear fibers to an array of small Winston cones located at the image plane. Working in the visible portion of the Cherenkov spectrum rather than the UV, this approach has several advantages:

- The coupling optical fibers can enter the radiator-gas volume, so that no additional windows are required.
- The mirrors do not have to work in the UV part of the spectrum.
- Requirements for radiator-gas purification are substantially eased.
- Partial instrumentation is easy, so that a phased construction plan can be followed.
- The shape of the detector plane can be optimized to reduce aberrations and astigmatism.

The obvious drawback is that no such device has yet been built. However, any problems associated with VLPCs will have to be solved for other parts of the spectrometer.

II.3 RICH Cost estimates

The major cost will be for readout electronics. A VLPC with its electronics, mechanics, and cryogenics is estimated to cost about \$50. Thus the readout cost would be ≈\$0.5M (10k channels x \$50/channel). We estimate the cost of the detector itself at ≈\$0.4M; this includes photon-detector hardware and mounts, mirrors, radiator box, gas system and monitoring equipment. It will be important to monitor temperature, pressure, and index of refraction of the radiator gas. Light sources will also be useful to allow monitoring of the photon detector.

If the CsI-photocathode chamber is chosen, the reduced cost of the readout will be offset by the necessity of quartz windows and higher detector construction cost. Thus, the cost of the detector will likely remain in the above range unless fewer pads are instrumented.

APPENDIX III: OPTICAL TRIGGER DESIGN CONSIDERATIONS

III.1 Introduction

Following a recent suggestion [1], we propose to use as pretrigger of the experiment a portion of a spherical crystal shell centered on the middle of the production target. The crystal, of refractive index n_1, is surrounded by a medium of refractive index n_2. Appropriate choices of refractive indices satisfy $n_1^2 - n_2^2 = 1 - \epsilon$, with ϵ positive and close to 0 (e.g. $n_1 = \sqrt{2}$ for a single crystal surrounded by air or vacuum). The crystal has the interesting capability of selecting in very short time (ns range) only those Cherenkov photons produced in the crystal by a charged particle having an impact parameter with respect to the center of the target larger than a threshold value b_{min}. The quantity b_{min} depends only on the crystal properties and can be tuned, as illustrated in Figure III.1.

Feasibility studies were performed during 1992 at Fermilab [2] using a flat MgF_2 crystal and at CERN [3] with a 100-mm-radius spherical shell of LiF of 3-mm thickness and 60-mm aperture. The results are encouraging: the crystal indeed functions as a fast impact-parameter band selector, with both upper and lower cutoffs tunable. The lower cutoff is adjusted by an appropriate choice of the parameter ϵ defined above, the upper cutoff by collimation of the output light. Figure III.2 shows the collected signal, obtained with a photomultiplier, as a function of the impact parameter of the incident charged particle. The measured shape is in good agreement with Monte-Carlo simulations. For small impact parameters, the background level is seen to be quite low, of order a few percent. The average number of photoelectrons for impact parameters below 2 mm is however too low for high-efficiency beauty-event selection using this first prototype.

A research and development proposal [62] was accepted by CERN in autumn 1992 with the goal of improving the sensitivity of the optical discriminator in the 0.3- to 1-mm impact-parameter range and to study the associated background. For beauty-event selection one needs to improve on past results with respect to both the threshold and slope of the signal as a function of impact parameter. The impact parameter threshold is given by

$$b_{min} = \epsilon \cdot R/2n_2, \tag{1}$$

where R is the radius of the crystal sphere and n_2 the refractive index of the coating material. Generally, within the visible spectrum ϵ is an increasing function of wavelength, thus the threshold b_{min} can be adjusted using a filter which retains only those photons with energy lower than E_{max} defined by $\epsilon(E_{max})=0$. Of course E_{max} should be within the sensitivity range of the photodetector. At low impact parameter the signal is small, thus a detector having good single-photoelectron response is needed. So far only photomultiplier tubes have been used; their characteristics are compared in Table III.1 with the very promising VLPCs [8], which have much higher quantum efficiency and localisation capability.

TABLE III.1 Comparison between photomultiplier and VLPCs

	Photomultiplier [b]	VLPC
Wavelength range [nm] [a]	200-500	400-800
Average quantum efficiency [%]	20	>50
Single-p.e. FWHM resolution [%]	66	<35
Single-p.e. dark count rate [kHz]	0.1	10

[a] Range within which the quantum efficiency exceeds 50% of its maximum value
[b] Hamamatsu R2059 with bialkali photocathode of type 400S

The threshold behavior of the crystal response is very sensitive to the variation of ϵ within the sensitivity band δE of the photodetector. Assuming a linear variation of ϵ with photon energy one can define an impact parameter $b_M = \epsilon(E_{min})R/2n_2$, E_{min} being the low-energy edge of the sensitivity band of the photodetector. The average number of photoelectrons N_{pe} produced by a particle with impact parameter b larger than an effective impact parameter threshold b_{eff} is then approximately given by

$$N_{pe} = K(b - b_{eff}), \tag{2}$$

where $b_{eff} = 0.78\,(b_{min} + b_M)$ and the constant K is given by the relation

$$K = 11.78\frac{(n_1^2 - 1)\delta E Q_e C_e}{n_1^2 n_2}\,. \tag{3}$$

K (in [mm^{-1}]) depends on the crystal refractive index, the photodetector quantum efficiency Q_e, the available bandwidth δE (in [eV]), and the light collection efficiency C_e. This simple relation is valid as long as the impact parameter does not exceed the crystal thickness. At higher impact-parameter values the number of photoelectrons first saturates and then (due to a drop in collection efficiency) diminishes; the drop in collection efficiency for large impact parameters is designed to suppress backgrounds due to delta rays and strange-particle decays. (At low impact parameters, this relation is only approximate, in that it considers the photoelectron yield to be zero up to b_{eff}; this is a convenient approximation for comparing various crystals, but in fact between b_{min} and b_{eff} the signal is not zero but averages about 10% of its value at $b = 2b_{eff}$.)

TABLE III.2 Performance of various radiator materials

	LiF [a]	Sapphire/Quartz	Sapphire/CCl_4
Readout	Mirror/PM	Fibers/VLPC	Fibers/VLPC
Radius [mm]	100	50	50
Filter [nm]	305	600	400
b_{min} [mm]	0.75 [b]	0.08 [b]	0.08 [c]
b_M [mm] [d]	2.75	0.28	0.24
Effective band width [eV] [e]	1.5	0.52	1.0
Average quantum efficiency assumed [%]	20	55	55
Collection efficiency [%]	28 [f]	80	80
b_{eff} [mm]	2.75	0.28	0.25
K [mm^{-1}]	0.45	1.3	2.5
N_{pe}/track/layer @ $b = 2b_{eff}$	1.24 [g]	0.36	0.63
N_{pe}/track/layer @ $b = (b_{min} + b_{eff})/2$	0.15	0.04	0.07
N_{pe}/track @ $b = 2b_{eff}$ (4 layers)	–	1.44	2.52

[a] Existing and tested LiF crystal 3mm thick

[b] Can be adjusted by a proper choice of the filter

[c] Can be tuned by adjustement of the temperature of the cladding CCl_4 fluid

[d] Given by the ϵ variation within the effective bandwidth

[e] Given by the high-wavelength limit of the quantum-efficiency curve

[f] This low value results from the poor reflectivity (35%) of the mirror used

[g] Measured value 1.23

In Table III.2 we compare the characteristics of the tested LiF crystal with two promising couples of core and coating materials: sapphire/quartz and sapphire/liquid-CCl_4. The crystal radius has been taken to be 50 mm (which improves the sensitivity by a factor of two relative to the 100-mm prototype tested at CERN, whose performance is also indicated in the Table), and we use VLPCs as the photodetector. We emphasize that no special development is needed to realize such a device; it can be constructed right now using known technology. The simple configuration of sapphire with pure quartz cladding, while attractive from the viewpoint of simplicity of construction and installation, is approximately a factor two less efficient than the combination sapphire/CCl_4. A test undertaken to improve the ϵ achromaticity domain of the sapphire/quartz couple by doping the quartz has not yet been successful. Moreover, the liquid-cladding configuration is advantageous and flexible, since the refractive index can be easily adjusted to its optimal value by either adding small quantities of a second liquid or by varying the temperature. One can tune the chromaticity of the system in the large-wavelength domain, as well as the value of the minimum impact parameter. For sapphire/CCl_4 one expects a variation of the threshold of 200 to 300 μm per °C. The sapphire/CCl_4 combination will be tested at CERN this year with both phototube and VLPC readout.

A further improvement can be obtained by replacing the single shell by 4 or 5 sub-shells

with the same total thickness. For impact parameter up to the thickness of the sub-shell the average number of photoelectrons should be multiplied by the number of sub-shells. Table III.2 shows that for a 4-layer device, an average of 2 – 3 photoelectrons per particle with 500-μm impact parameter is well within reach. As shown in Section III.4, this should suffice for efficient triggering on beauty.

III.2 Crystal design and backgrounds

A four- or five-subshell device with liquid coating is suitable for the proposed experiment (see Section III.4). The liquid coating is thin and represents only a small fraction of the total thickness of the device. The crystal has a hole in its center to let the beam pass through. The diameter of the hole is a compromise between the acceptance of the device and the level of background associated with beam halo particles crossing the crystal. We are considering a hole of 1 mm, diameter, giving an acceptance cutoff at 10 mr for a 50-mm-radius crystal. More work is needed to estimate the halo-induced background with such a hole size.

The average number of photoelectrons in the range of impact parameter between b_{min} and b_{eff} is about 10% of the number of photoelectrons for an impact parameter $2b_{eff}$. A good efficiency for charged particles arising from beauty decay, with average impact parameter of about 600 μm, cannot be achieved without some sensitivity of the device for particles with 100- to 200-μm impact parameter. It is therefore important to maintain the target size as small as possible such that most of the impact parameters associated with the dispersion of the primary vertex inside the target will be kept below a few hundred μm. This is realised with a target that does not exceed 300 μm transversely and has a thickness of up to 2 mm along the beam.

The remaining backgrounds arise from multiple reflections to the edge of the crystal of light which should normally be refracted out of the crystal, delta rays or nuclear interactions produced in the crystal by particles from the primary vertex, and production and decay upstream of the crystal of strange particles.

III.3 Trigger scheme

Since the optical discriminator is very fast it can be used as a first-level trigger. We plan to achieve a rejection factor of about 100 for minimum-bias events while keeping about 40% of the produced beauty events. This will be realised in two steps. The first step is based on a threshold imposed on the total number of photoelectrons detected. This functions as a combined charged-particle-multiplicity and impact-parameter trigger. It will provide a reduction factor of order 10 for minimum-bias events and a beauty efficiency above 60%. In the second step we take advantage of the granularity of the VLPC photodetector to reject background events according to topological criteria. This second part of the trigger is presently under study, with two options under consideration.

In a first option, light-collecting optical fibers at the edge of the crystal are arrayed on a cone whose apex coincides with the average virtual source of the outgoing photons. This solution requires about 600 VLPC channels and provides a measurement of the azimuthal angle of the outgoing photon. Photons belonging to the same particle tend to group within a

sector of 10 to 20 degrees; for example the two charged particles from a two-prong decay will tend to produce two groups of photons detected at azimuthal angles 180° apart. Requiring at least two distinct groups of photons will greatly reduce the background without much affecting the efficiency for beauty events.

A more ambitious option places the fibers farther from the crystal edge, with an appropriate optical system inserted in between so as to get also information on the angle of the photon with respect to the normal to the exit face. This option might require up to an order of magnitude more VLPC channels, but in principle one would be able to reconstruct the entire image, determine the impact parameter with more precision, and to some extent determine the location of the crossing point of the particle inside the crystal. The contributions to the resolution on these quantities due to the variation of the Cherenkov opening angle with photon wavelength, the crystal thickness, the geometrical constraints, and chromatic aberrations at the exit are not yet sufficiently understood to conclude whether such an option is worthwhile.

III.4 Monte Carlo simulation

We have simulated the response of a 4-layer device consisting of spherical sapphire shells of 0.4-mm thickness, each with diameter of 30 mm and radius of curvature of 50 mm. The spacing between the crystals is 0.1 mm and is filled with pure CCl_4 liquid. The total thickness of the device is 0.7 g/cm^2 and represent 0.7% interaction length and 2.5% radiation length. The central hole in the device has a diameter of 1 mm. The angular coverage is from 10 to 300 mr. We assume a cylindrical gold or tungsten target 200 μm in diameter and 2 mm in thickness and an interaction rate of 100 Mhz. As photodetector we assume VLPCs coupled to the crystal through optical fibers with double cladding and large numerical aperture. The threshold on each VLPC discriminator is set at 0.5 photoelectron. The fiber arrangement corresponds to the first option described above. The simulation includes most known effects, including pileup of events from multiple interactions, but at this point includes neither the interaction of halo particles with the device nor secondary nuclear interactions inside the device. We use the PYTHIA event generator from the Lund Monte Carlo. The results are presented in Figure III.3, where the efficiencies for minimum-bias, charm, and beauty events (with one B decaying in the $\pi^+\pi^-$ channel and the other decaying at random) are plotted as a function of the threshold applied to the total number of photoelectrons detected.

APPENDIX IV: RESULTS FROM OPTICAL-TRIGGER TESTS

Attached are two recent preprints describing the first tests of the principle of the optical impact-parameter trigger.

References

[1] G. Charpak, L. M. Lederman, and Y. Giomataris, Nucl. Instr. & Meth. **A306**, 439 (1991).

[2] D. M. Kaplan *et al.*, "Test of Principle of an Optical Trigger for Beauty," FERMILAB-Pub-93/002, to appear in Nucl. Instr. & Meth. (1993).

[3] G. Charpak *et al.*, "Experimental Study of an Impact-Parameter Optical Discriminator", CERN-PPE/93-14, submitted to Nucl. Instr. & Meth. (1993).

[4] D. M. Kaplan and B. Lundberg, "Prospects for Fixed-Target Beauty Physics in the Main-Injector Era," in **Fermilab Program through 1997 and Beyond,** supplemental materials submitted to the 1992 HEPAP Subpanel, pp. 7-4 to 7-7, February 1992.

[5] Y. Giomataris, "Comments on the Future of B Physics in Hadron Machines," unpublished, 1992.

[6] J. S. Kapustinsky, "Radiation Damage Effects on the Silicon Microstrip Detector in E789 - A Fixed Target Experiment at Fermilab," *International Conference on Advanced Technology and Particle Physics*, Como, Italy, June 22–26, 1992.

[7] C. Lee *et al.*, "A Parallel Pipelined Dataflow Trigger Processor," *IEEE Trans. Nucl. Sci.* **38**, 461 (1991).

[8] M. Atac *et al.*, Nucl. Instr. & Meth. **A320**, 155 (1992).

[9] M. Atac *et al.*, Nucl. Instr. & Meth. **A314**, 56 (1992).

[10] H. Albrecht *et al.*, "An Experiment to Study CP Violation in the B System Using an Internal Target at the HERA Proton Ring," Letter of Intent to DESY, W. Hofmann and W. Schmidt-Parzefall, spokespersons, October 1992.

[11] C. Albajar *et al.*, Phys. Lett. **209B**, 397 (1988); H. Albrecht *et al.*, Phys. Lett. **199B**, 451 (1987); P. Avery *et al.*, Phys. Lett. **223B**, 470 (1989).

[12] See for example C. Albajar *et al.*, Phys. Lett **262B**, 163 (1991) and D. Cline, "Recent Results on the Search for Flavor-Changing Weak Neutral Currents and $B^0 - \bar{B}^0$ Mixing," UCLA-PPH-31-5-91-DBC, invited talk given at the 3rd Topical Seminar on Heavy Flavors, San Miniato, Italy, June 17–21, 1991.

[13] D. Cassel, "b Physics," Cornell preprint CLNS 93/1190, January 1993, to appear in *Proceedings of the 7th Meeting of the American Physical Society Division of Particles and Fields (DPF92)*, Fermilab, November 10–14, 1992; see also B. Adeva *et al.*, Phys. Lett. **252B**, 703 (1992).

[14] F. Abe *et al.*, Phys. Rev. Lett. **67**, 3351 (1991).

[15] B. Grinstein, M. Savage, and M. Wise, Nucl. Phys. **319B**, 271 (1989) and B. Grinstein, R. Springer, and M. Wise, Nucl. Phys. **337B**, 269 (1990).

[16] See for example and a list of references A. Ali and C. Greub, Z. Phys. **C49**, 431 (1991) and Phys. Lett. **259B**, 182 (1991); also A. Ali and C. Greub, "Rare Decays $B \to X_d+\gamma$ in the Standard Model," DESY preprint 92-048, March 1992.

[17] See for example N. G. Deshpande *et al.*, Phys. Rev. **D39**, 1461 (1989).

[18] A. Ali, T. Ohl, and T. Mannel, Phys. Lett. **298B**, 195 (1993).

[19] J. S. Hagelin, S. Kelley, and T. Tanaka, "Supersymmetric Flavor Changing Neutral Currents: Exact Amplitudes and Phenomenological Analysis," MIU-THP-92-59, submitted to Nucl. Phys. B (1992).

[20] G. Crawford, "Search for Rare B Decays in CLEO," Fermilab seminar, March 9, 1993.

[21] I. I. Bigi and B. Stech, in *Proceedings of the Workshop on High Sensitivity Beauty Physics at Fermilab, Fermilab, Illinois, November 11–14, 1987*, edited by A. J. Slaughter, N. Lockyer, and M. Schmidt (FNAL, 1988).

[22] M. Gronau, Phys. Lett. **300B**, 163 (1993).

[23] H. Castro *et al.*, "Expression of Interest for a Bottom Collider Detector at the SSC," SSCL-SR-1163, May 1990.

[24] M. Wirbel, Nucl. Phys. B, Proc. Suppl. 13, 435 (1990).

[25] I. Dunietz, "CP Violation with Additional B Decays," in **B Decays**, S. Stone, *ed.*, World Scientific, Singapore, 1993, p. 393, and references therein.

[26] L. Wolfenstein, Phys. Lett. **164B**, 170 (1985).

[27] S. Barlag *et al.*, Z. Phys. **C48**, 29 (1990) and Z. Phys. **C55**, 383 (1992).

[28] D. Cline, "The Continuing Search for Flavor-Changing Weak Neutral Currents," Comm. Nucl. Part. Phys. **16**, 131 (1986), and references therein.

[29] P. Colangelo, G. Nardulli, and N. Paver, Phys. Lett. **242B**, 71 (1990).

[30] J. C. Anjos et al., Phys. Rev. Lett. **60**, 1239 (1988).

[31] J. C. Anjos *et al.*, Phys. Rev. Lett. **62**, 1587 (1989).

[32] Sheldon Stone, HEPSY preprint 1-92, April 1992

[33] G. Crawford *et al.*, Phys. Rev. **D44**, 3394 (1991).

[34] R.M. Baltrusaitis *et al.*, Phys. Rev. Lett. **66**, 142 (1991).

[35] K. Kodama *et al.*, Phys. Rev. Lett. **66**, 1819 (1991).

[36] R.M. Baltrusaitis *et al.*, Phys. Rev. Lett. **54**, 1976 (1985).

[37] D. Coffman et *et al.*, Phys. Rev. **D45**, 2196 (1992).

[38] The E687 Collaboration, "Description and Performance of the Fermilab E687 Spectrometer," FERMILAB-Pub-90/258-E (1990).

[39] K. Kodama *et al.*, Phys. Lett. **263B**, 573 (1991).

[40] R. Ammar *et al.*, Phys. Rev. Lett. **61**, 2185 (1988).

[41] D. M. Alde *et al.*, Phys. Rev. Lett. **66**, 133 (1991).

[42] P. Nason, S. Dawson, and R. K. Ellis, Nucl. Phys. **303B**, 607 (1988); **327B**, 49 (1989); **335B**, 260 (1990).

[43] E. L. Berger, "Phenomenology of Heavy Quark Production," in *Proceedings of 9th Physics in Collision Conference, Jerusalem, Israel, June 19–21, 1989*, p. 101.

[44] D. M. Alde *et al.*, Phys. Rev. Lett. **66**, 2285 (1991).

[45] H. Albrecht *et al.*, Phys. Lett. **209B**, 119 (1988).

[46] C. Bebek *et al.*, Phys. Rev. Lett. **62**, 8 (1989).

[47] J. F. Arens *et al.*, H. Heijne *et al.*, S. Parker *et al.*

[48] P. E. Karchin, Nucl. Instr. & Meth. **A305**, 497 (1991).

[49] S. Parker, private communication.

[50] C. S. Mishra *et al.*, "Performance of a Silicon Microstrip Detector in a High Radiation Environment," *Proceedings of the 15th APS Division of Particles and Fields General Meeting*, Houston, TX, January 3–6, 1990.

[51] See for example R. Bouclier *et al.*, Nucl. Instr. & Meth. **A315**, 521 (1992) and references therein.

[52] M. Atac, Nucl. Instr. & Meth. **176**, 1 (1980).

[53] M. Atac, C. N. Kim, M. Mishina, and R. Ruchti, in preparation (1993).

[54] A. D. Bross and A. Pla-Dalmau, "Radiation Effects in Intrinsic 3HF Scintillator," FERMILAB-PUB-92-247, Oct. 1992, submitted to Nucl. Instr. & Meth. and A. D. Bross and A. Pla-Dalmau, "Radiation-Induced Hidden-Absorption Effects in Polystyrene-Based Plastic Scintillators," in **Radiation Effects on Polymers**, Proceedings of an ACS Symposium, R. L. Clough and S. W. Shalaby, *eds.*, American Chemical Society, Washington, DC, 1991, p. 578.

[55] P. Besser and M. D. Petroff, Rockwell International Science Center, private communication.

[56] M. G. Stapelbroek, M. D. Petroff, and R. Bharat, "Visible Light Photon Counters for Astronomy," to appear in *Proceedings of an ESA Symposium on Photon Detectors for Space Instrumentation*, ESA/ESTEC, Noordwijk, The Netherlands, 10–12 November 1992.

[57] M. D. Petroff and M. G. Stapelbroek, IEEE Trans. Nucl. Sci. **NS-36**, 163 (1989).

[58] B. Abbott *et al.*, Nucl. Instr. & Meth. **A327**, 319 (1993).

[59] J. T. Shank *et al.* Nucl. Instr. & Meth. **A309**, 377 (1991).

[60] G. Abshire *et al.*, Nucl. Instr. & Meth. **164**, 67 (1979).

[61] D. Muller, Phys. Rev. **D5**, 2677 (1972).

[62] G. Charpak *et al.*, "Study of an Optical Trigger to be used for Beauty search in fixed target mode at LHC", CERN-DRDC/RD30, 20th August 1991.

[63] R. Gomez *et al.*, Phys. Rev. **D35**, 2736 (1987).

[64] D. A. Stewart, Ph.D. thesis, Indiana University, May 1988.

[65] Y. B. Hsiung *et al.*, Nucl. Instr. & Meth. A245, 338 (1986) and references therein.

[66] M. Kreisler, private communication. This is an estimate of the actual time during which the processor was in use and excludes nights, weekends, holidays, and repair periods; the total calendar time was 6 months.

[67] S. Hansen, Fermilab, private communication; J. Lillberg, Los Alamos National Laboratory, private communication.

[68] D. M. Kaplan *et al.*, "Backgrounds to the Detection of Two-Body Hadronic B Decays," in *Proceedings of the Workshop on High-Sensitivity Beauty Physics*, A. J. Slaughter, N. Lockyer, and M. Schmidt, *eds.*, Fermilab, November 1987, p. 301; Fermilab Proposal 789, "Study of Two-Prong Decays of Neutral B Mesons and Λ_b," D. M. Kaplan and J. C. Peng, spokespersons, September 1988.

[69] J. C. Peng *et al.*, "Preliminary Results from Fermilab E789," FERMILAB-Conf-92/301, presented at the *XXVI International Conference on High Energy Physics*, Dallas, TX, August 6–12, 1992.

[70] E. L. Berger, "Heavy Flavor Production at Fixed Target and Collider Energies," Published in *Proceedings of the Storrs Meeting*, K. Haller, *et al., eds.*, World Scientific, Singapore, 1989, p. 497.

[71] S. Holmes and P. Martin, private communication.

[72] **B Factories, The State of the Art in Accelerators, Detectors and Physics**

[73] F. A. Jenkins and H. E. White, **Fundamentals of Optics**, McGraw-Hill, New York (1957).

[74] Klein, **Optics.**

[75] B. Hoeneisen, D. F. Anderson, and S. Kwan, Nucl. Instr. & Meth. A302, 447 (1991).

[76] S. Kwan and D. F. Anderson, Nucl. Instr. & Meth. A309, 190 (1991).

[77] D. F. Anderson *et al.*, FERMILAB-Conf-92/135, June 1992.

[78] B. Lund-Jensen, "Single-Photon Detectors for Cherenkov Ring Imaging," Ph.D. Thesis, published in **Acta Universitatis Upsaliensis, Comprehensive Summaries of Uppsala Dissertations from the Faculty of Science, 172**, Almqvist & Wiksell, Stockholm, 1988.

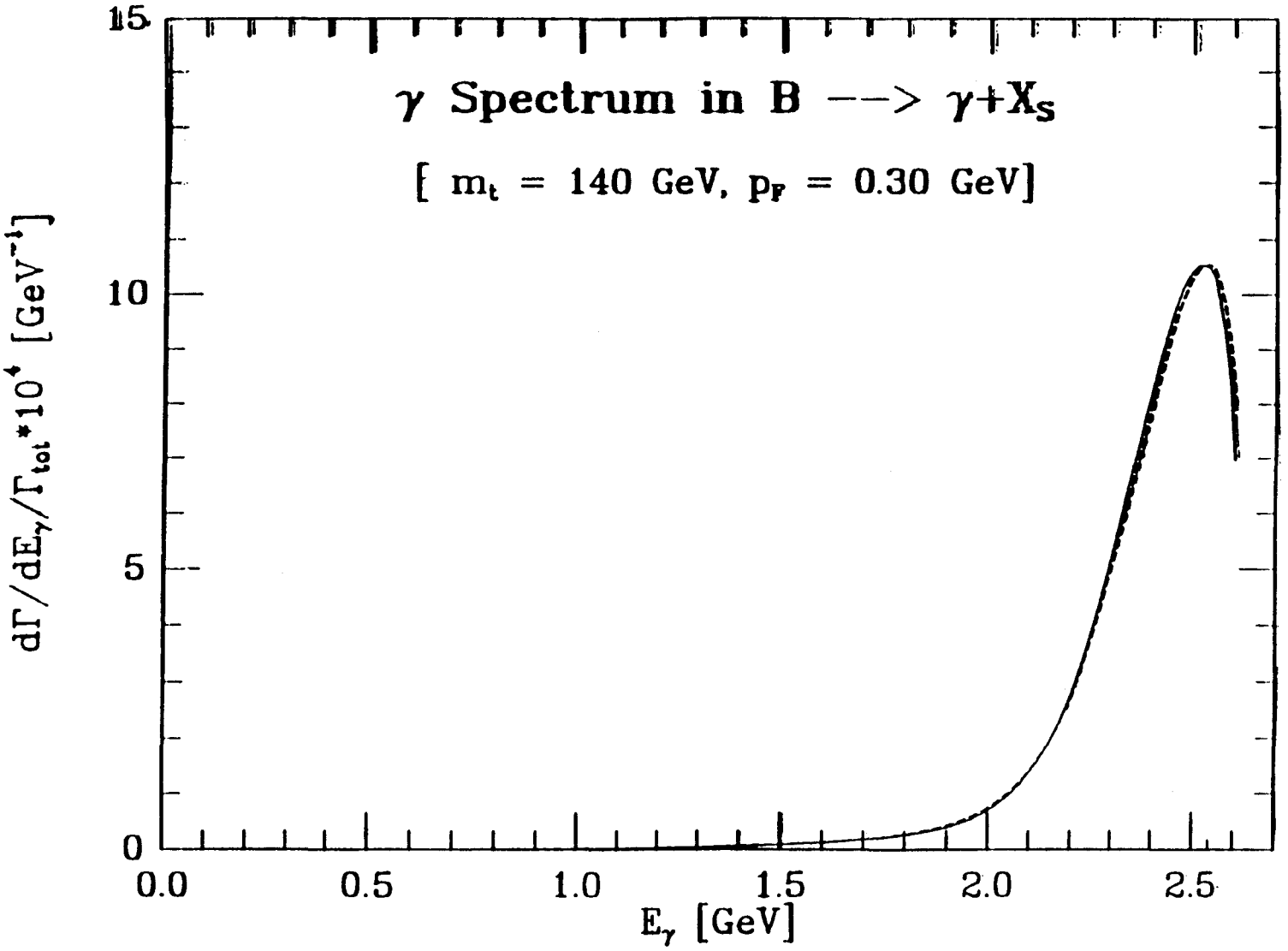

Figure 2.1 - Spectrum of the γ expected in $b \rightarrow s\gamma$ decays.

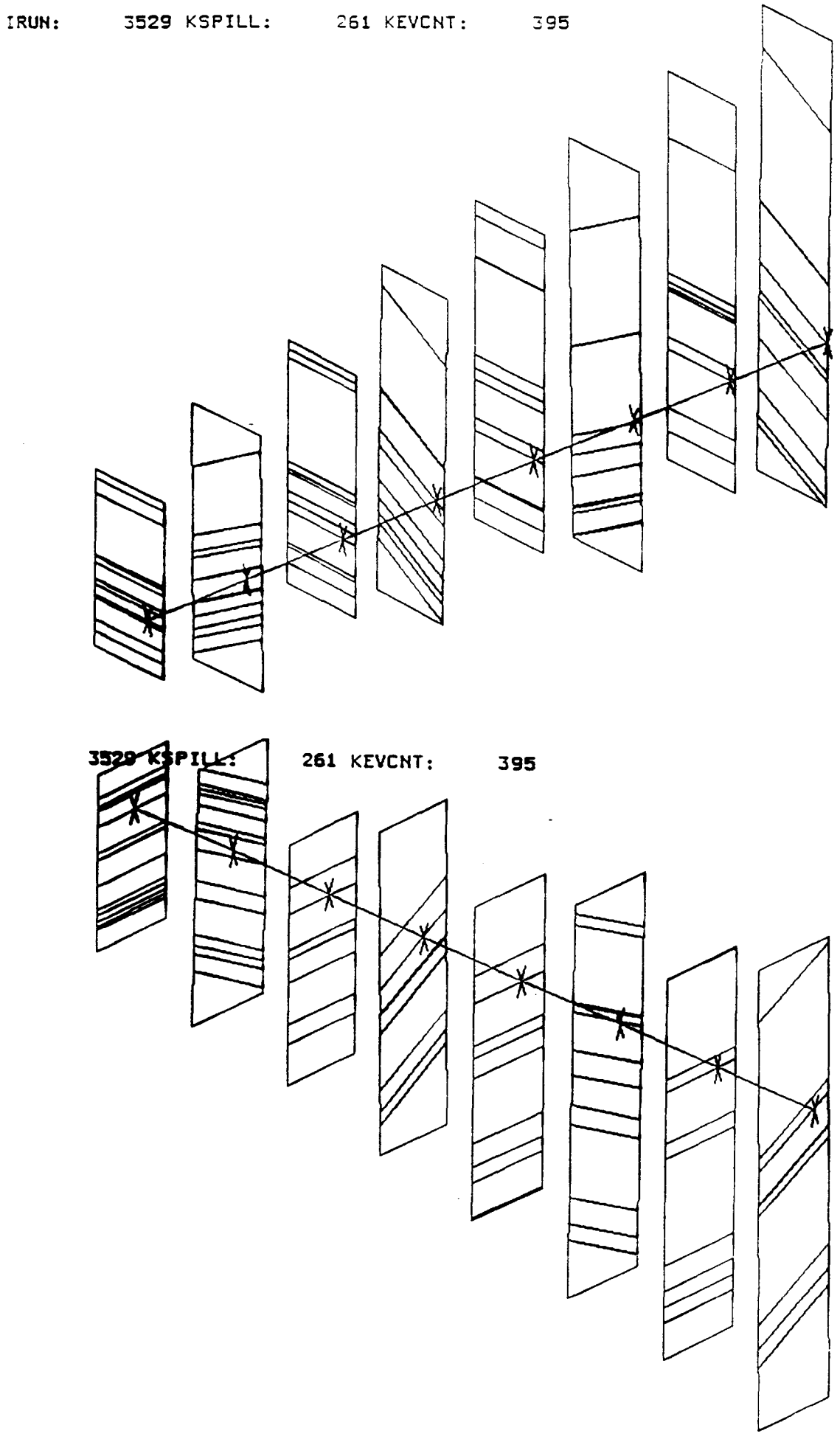

Figure 3.1 - Typical event from E789 obtained at an interaction rate of 50 MHz. The hit density in the silicon detectors is ≈20 hits per plane on average.

Silicon Vertex analysis

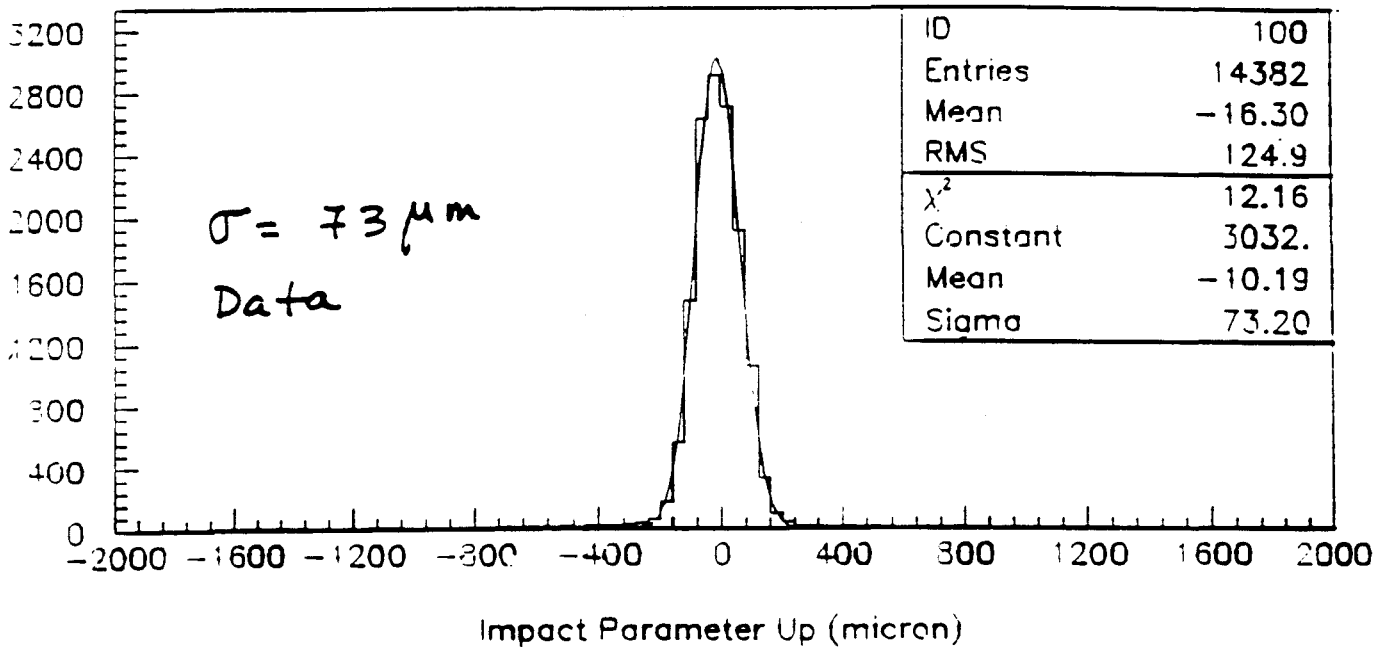

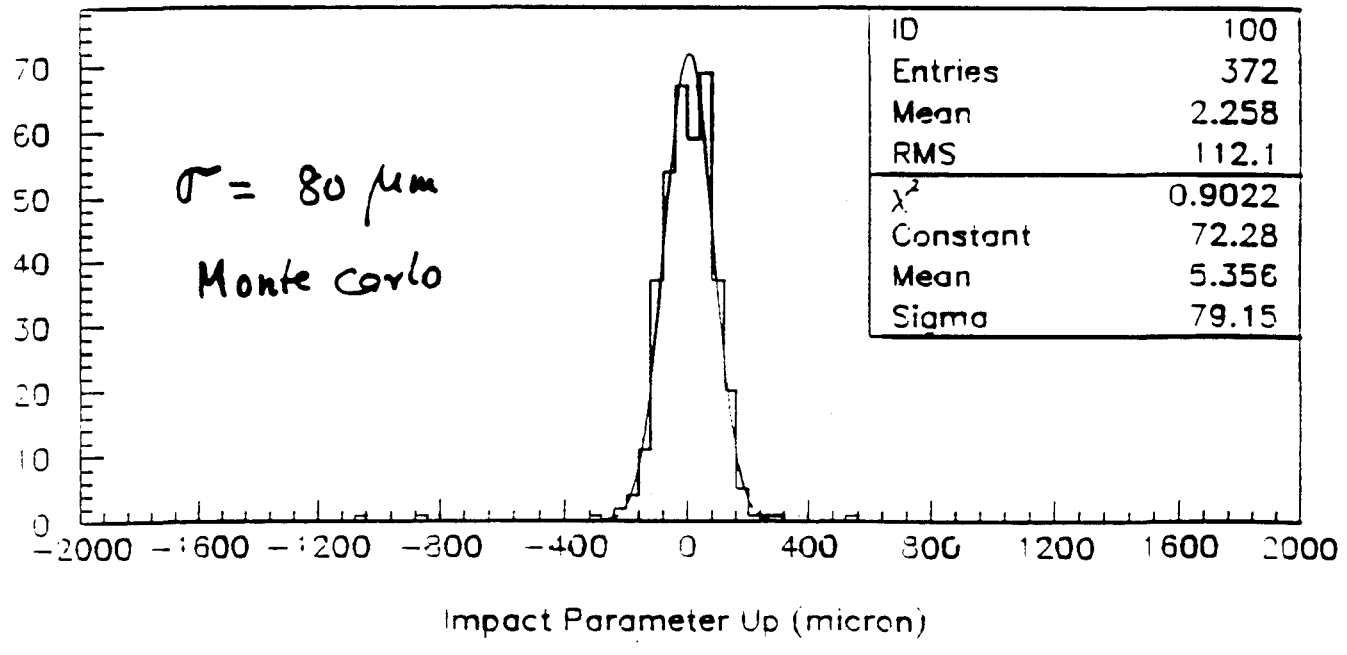

Figure 3.2 - the transverse position resolution achieved in E789 (the width is dominated by the contribution from the 200 micron high target).

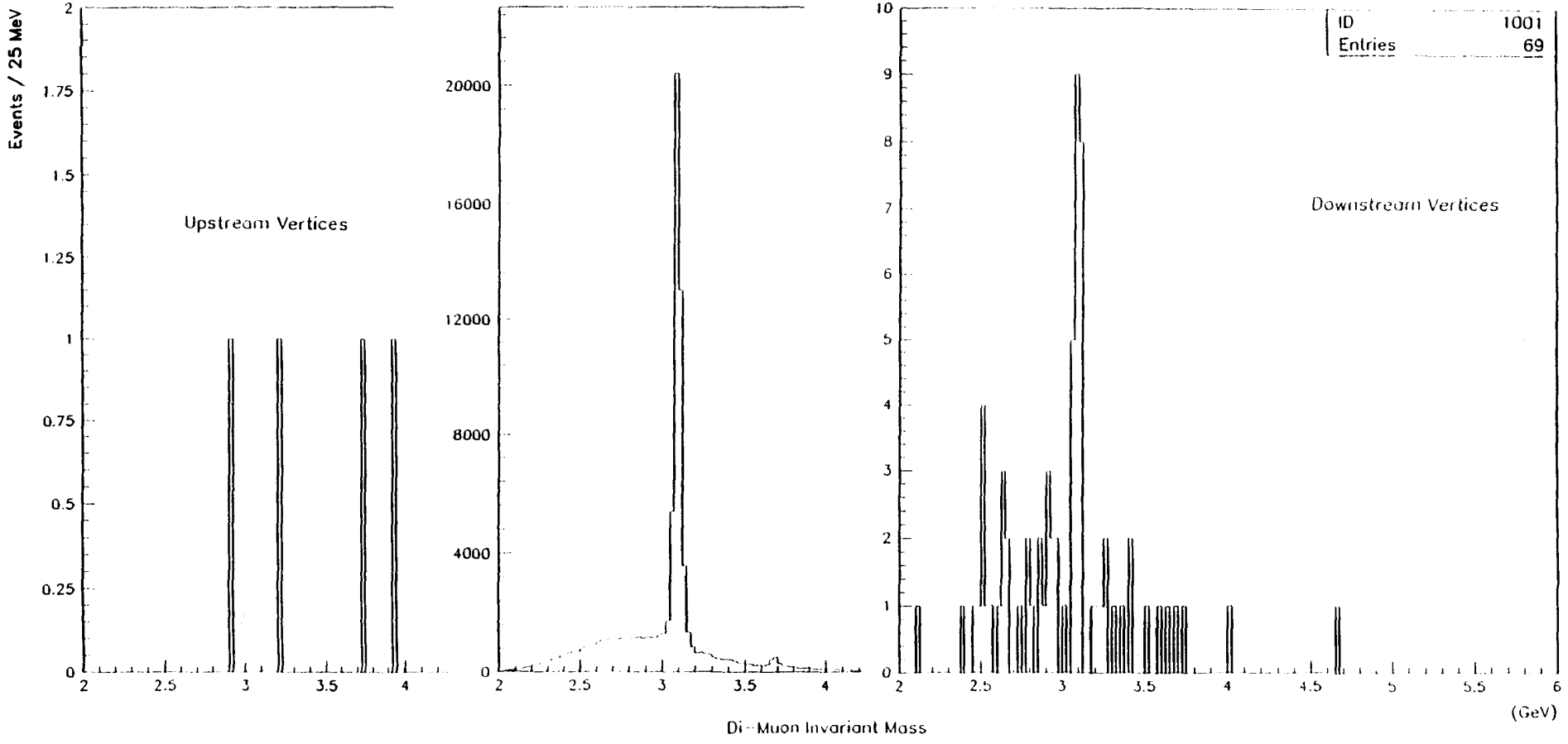

Figure 3.3 - the observed dimuon mass distributions for events with reconstructed vertex respectively: upstream of the target, inside the target volume, and downstream of the target; a clear $B \rightarrow J/\psi$ signal is evident.

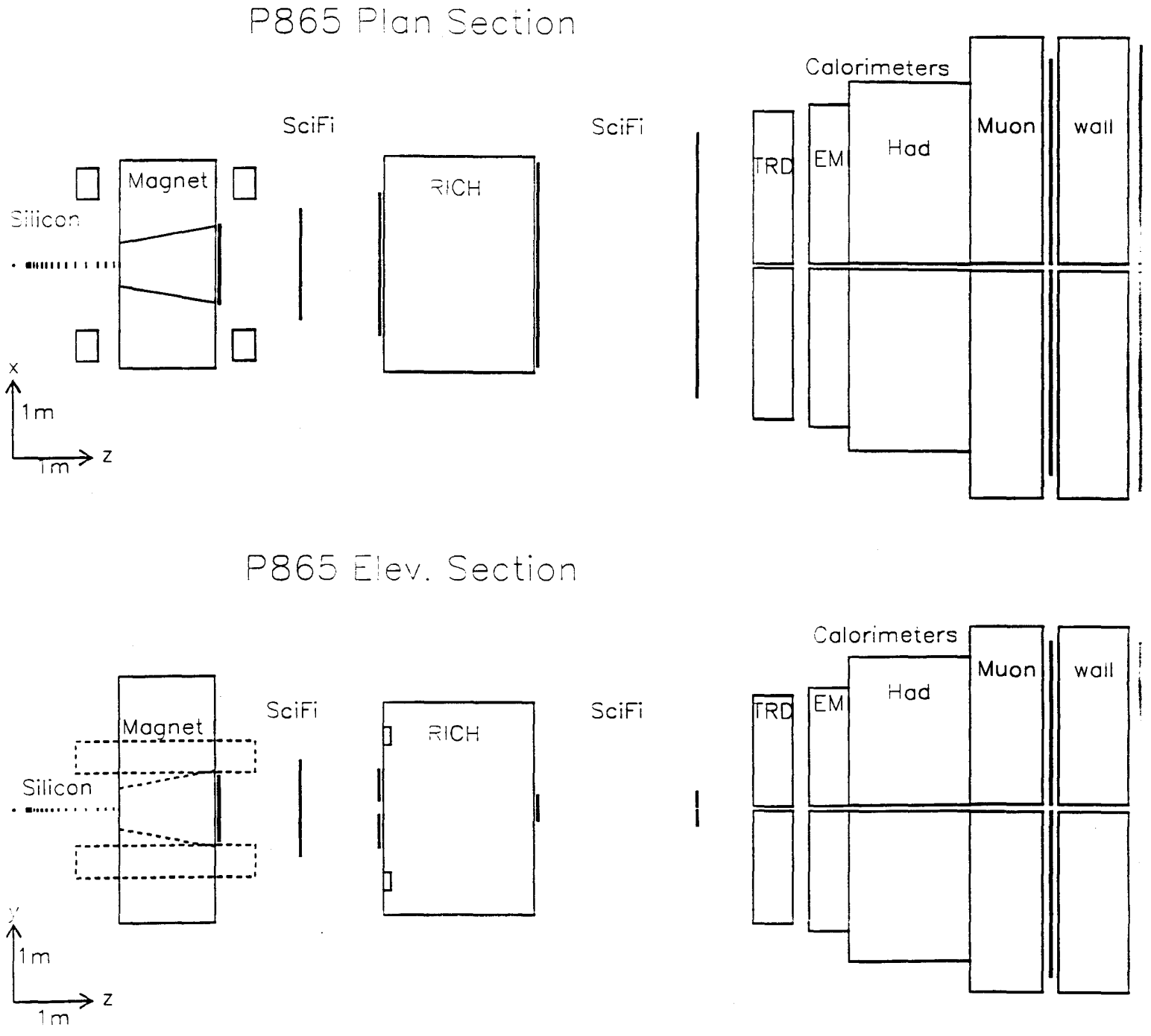

Figure 3.4 - the schematic layout of the proposed P865 spectrometer.

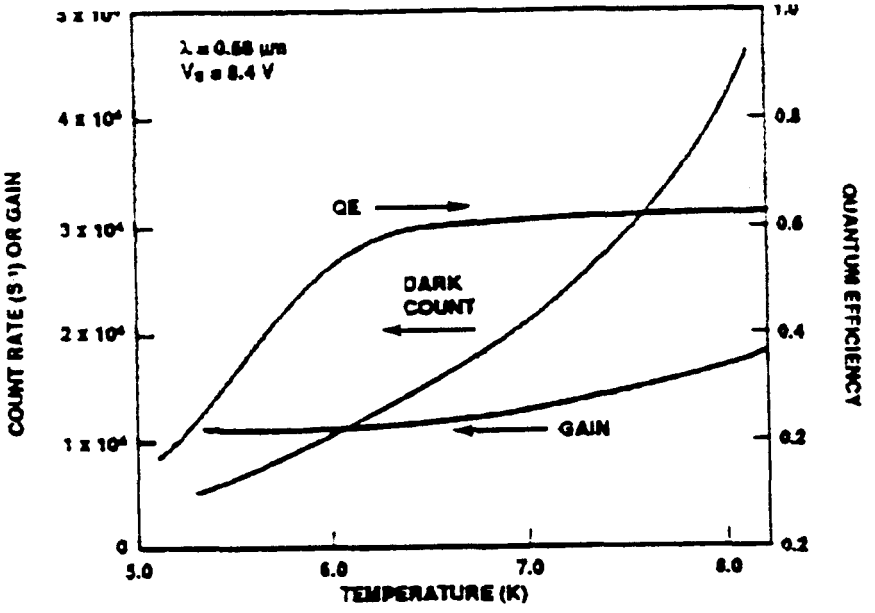

Quantum efficiency, gain, and dark count rate of a VLPC as functions of operating temperature.

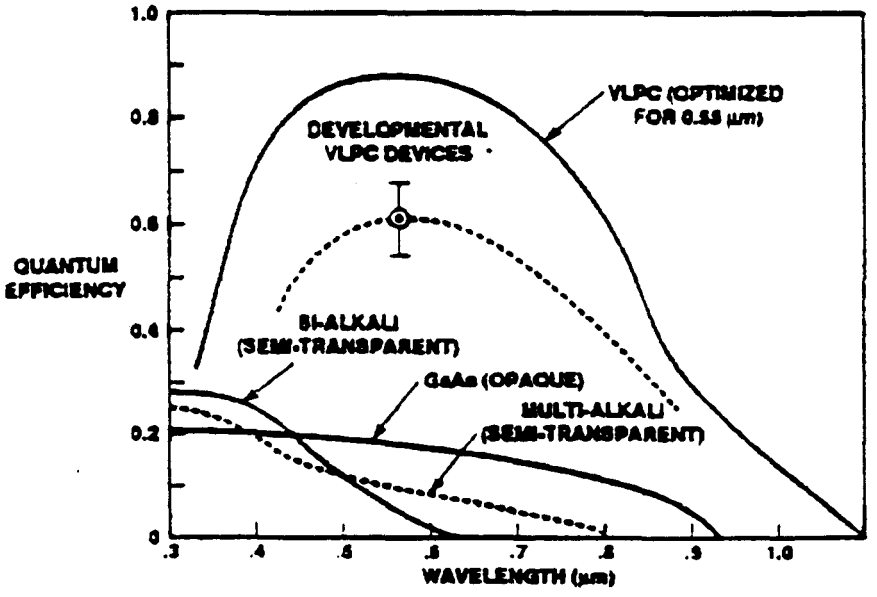

Quantum efficiencies for VLPCs compared to several common photocathodes. Improvements over current developmental VLPCs are expected to yield peak QEs near 0.9 for wavelengths near 0.55 micron.

Figure 3.5

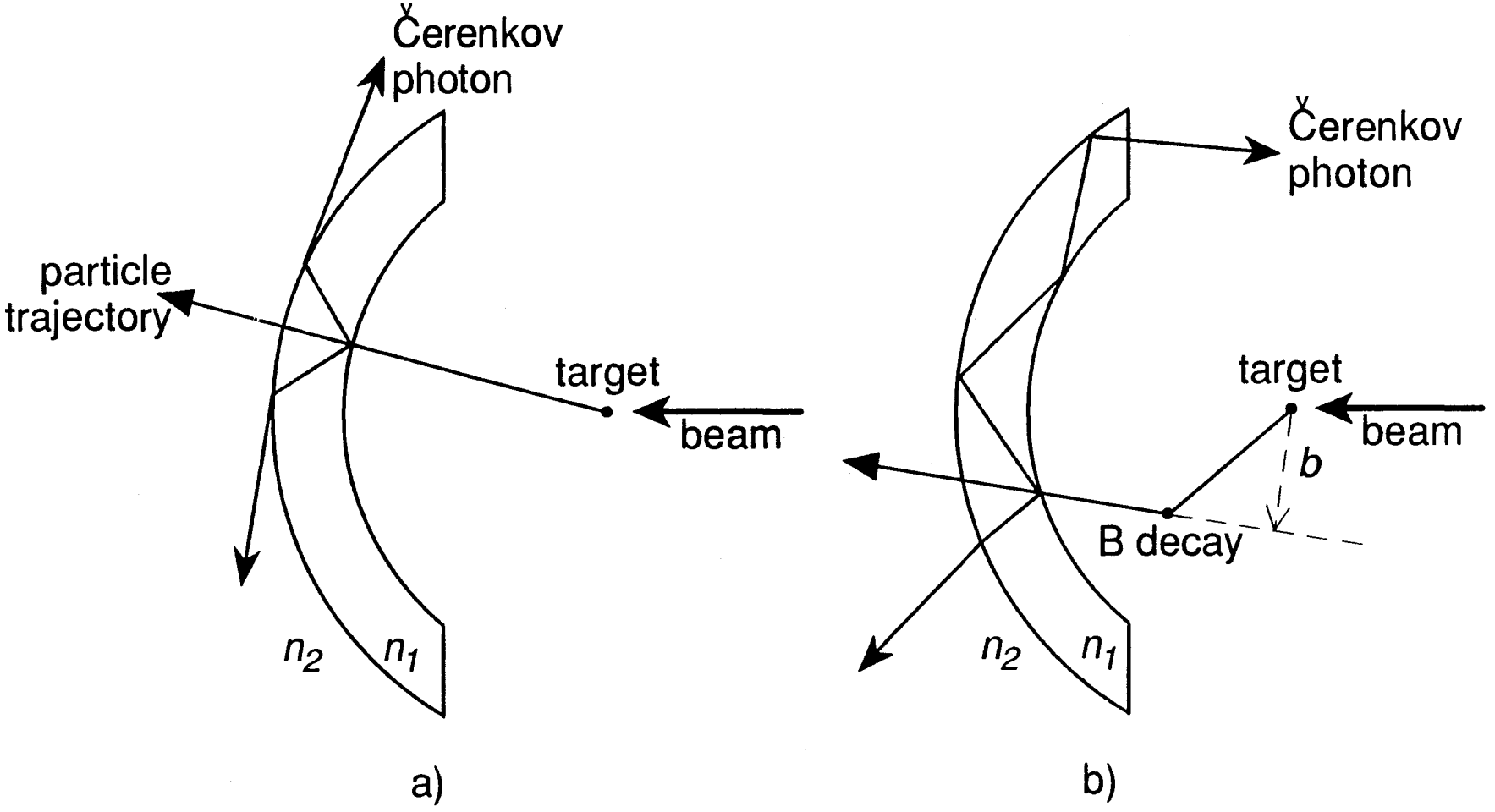

Figure 3.6 - Schematic of the optical trigger. The Cherenkov light from a target track escapes the crystal but light from a track of finite impact parameter is trapped and exits the rim of the crystal.

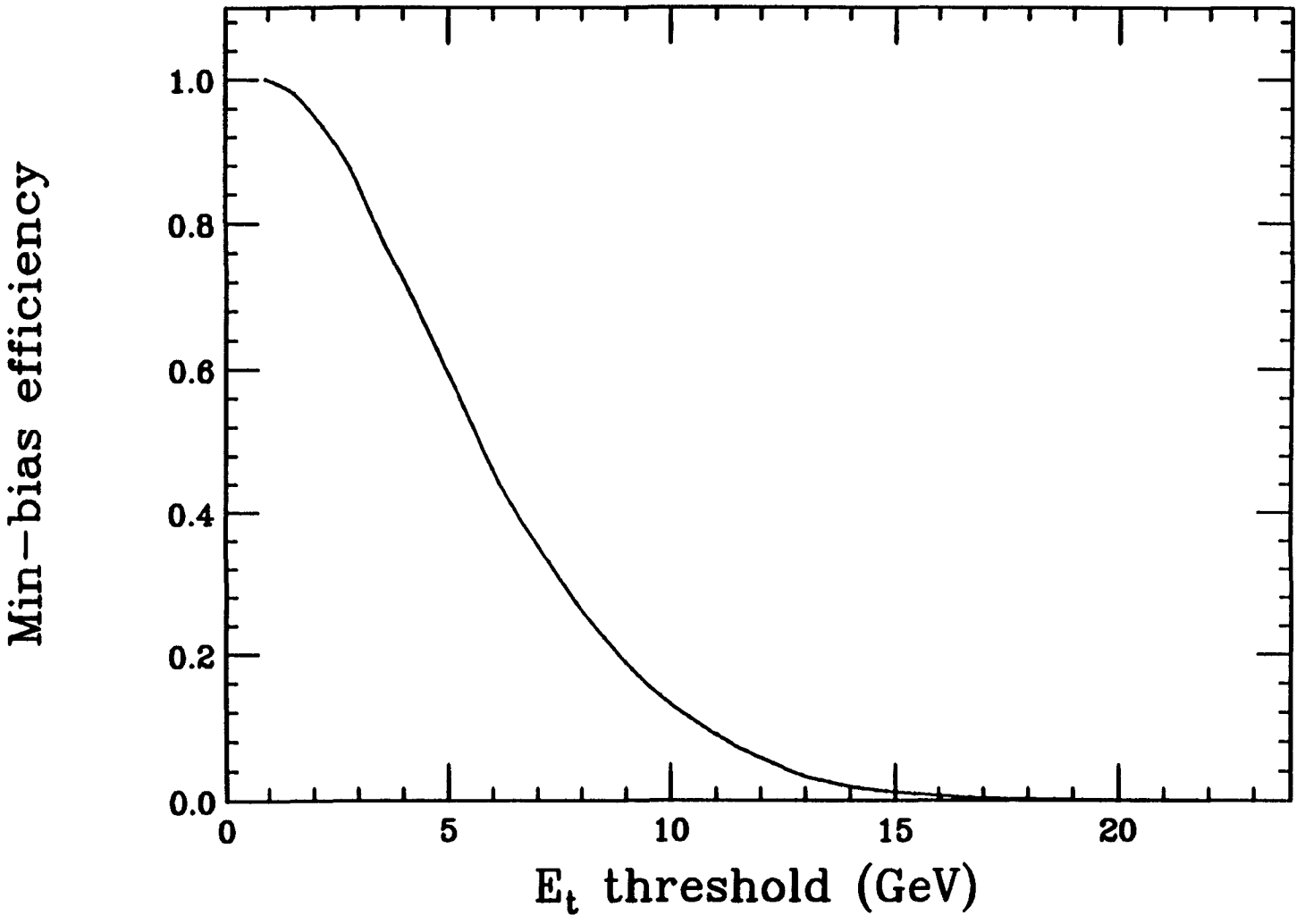

Figure 3.7 - Trigger efficiency for minimum-bias events vs. E_t threshold based on data from E557/672.

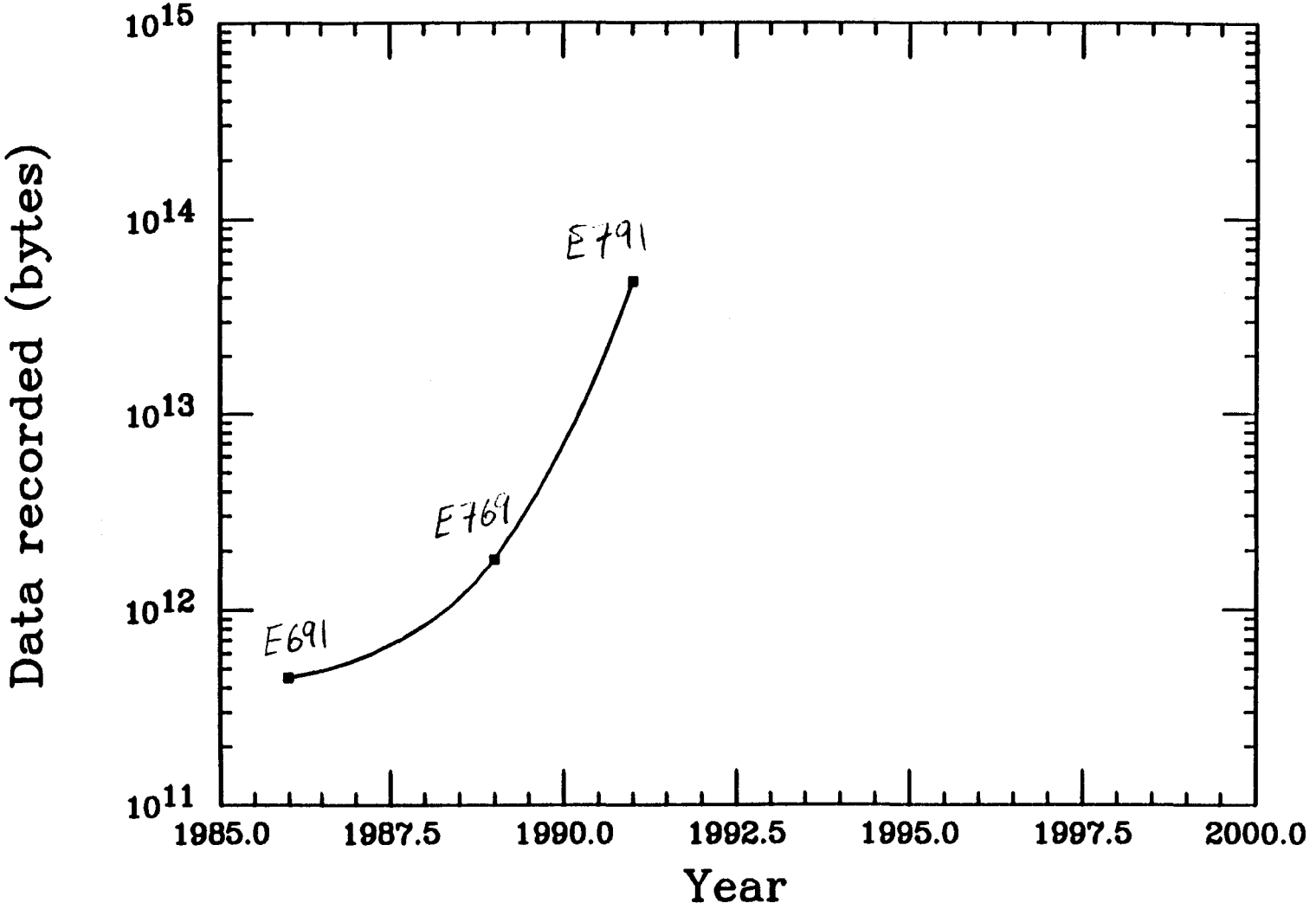

Figure 3.8 - Data recorded by fixed target charm experiments. It appears likely that by 1995 it will be practical to analyze $\sim 10^{15}$ bytes/year.

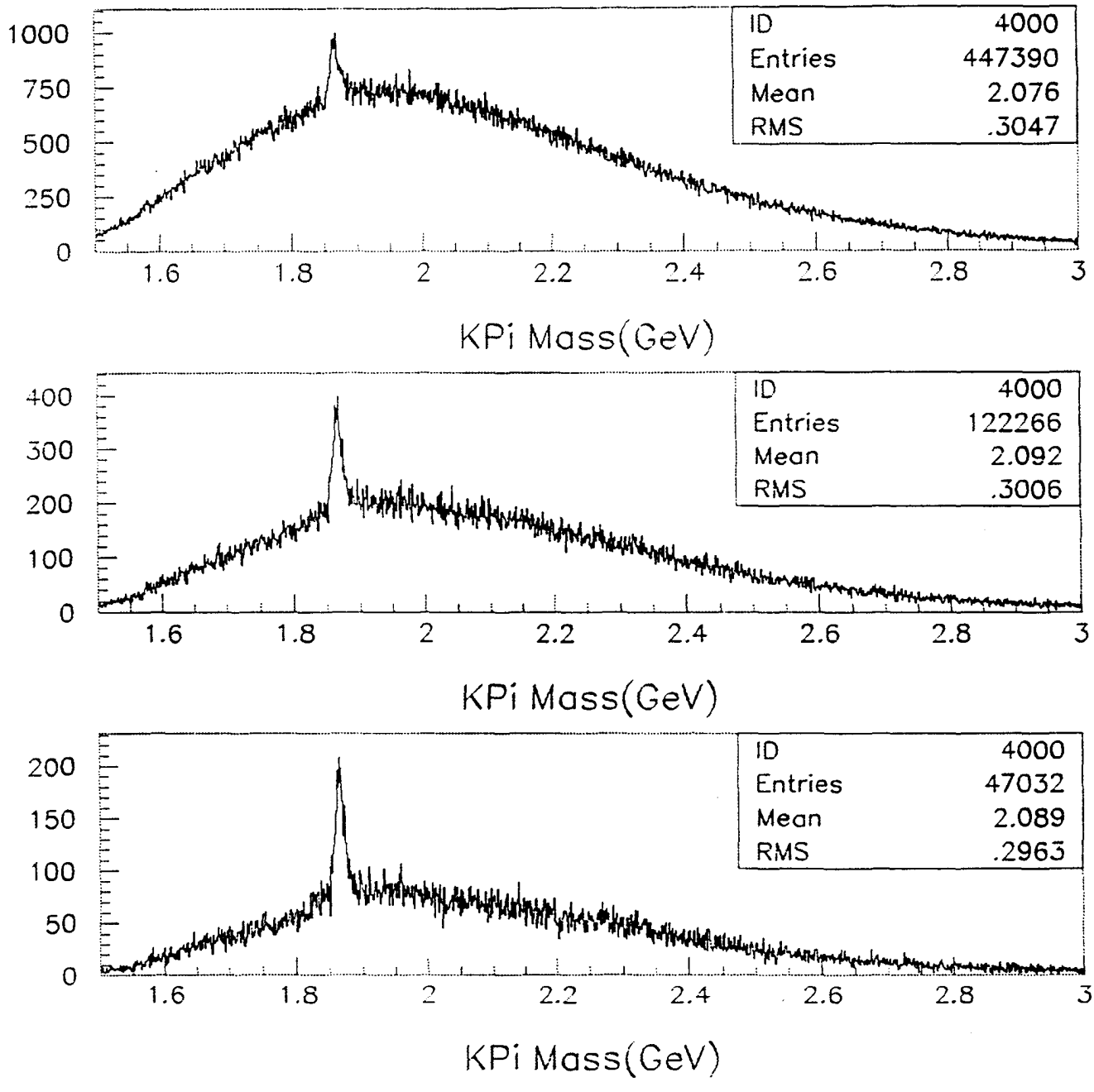

Figure 4.1 - Demonstration from E789 of the power of vertex cuts to suppress light quark backgrounds, in a geometry comparable to the one proposed. The curves correspond to successively tighter vertex cuts.

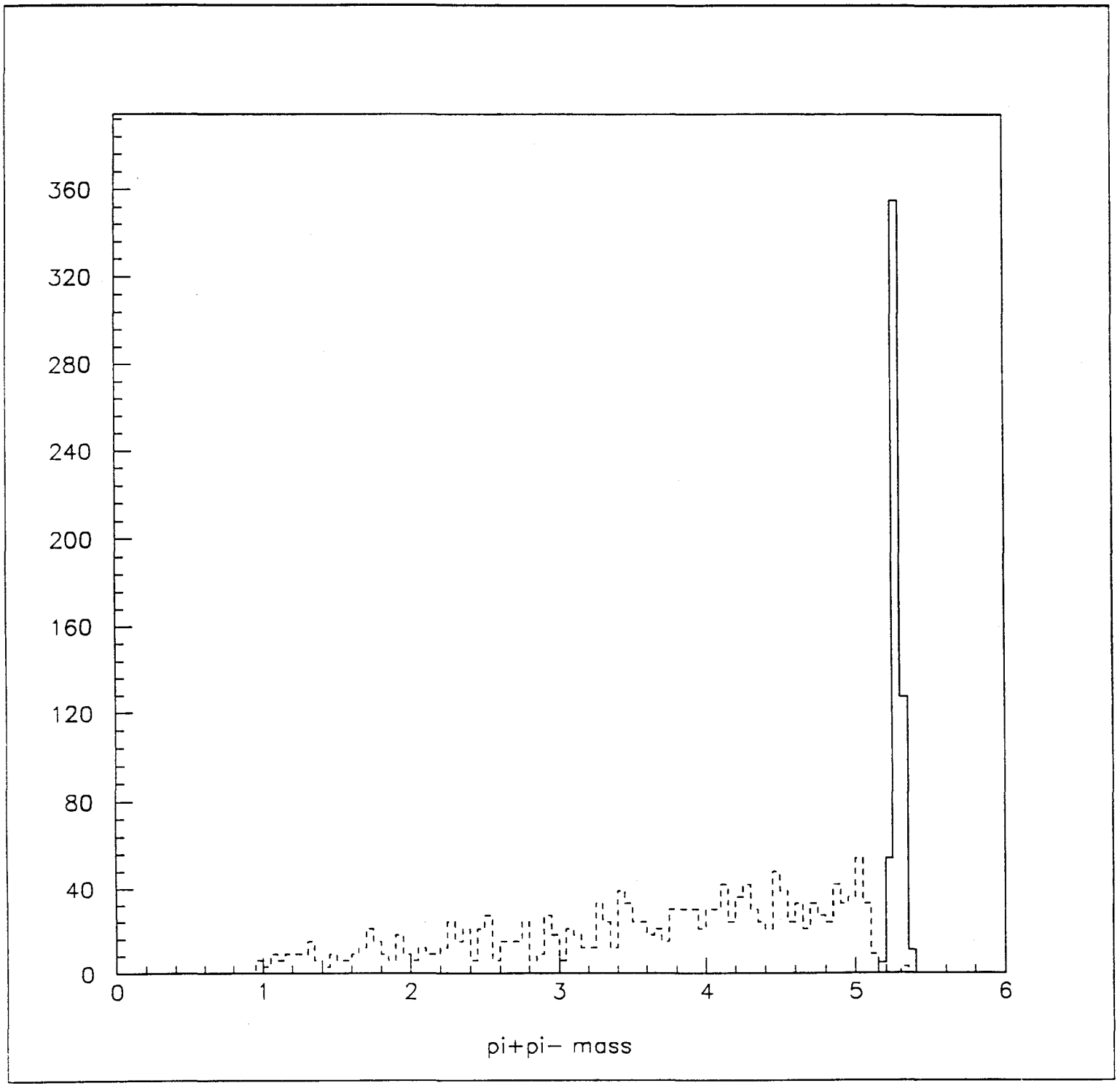

Figure 4.2 - The mass resolution of the proposed spectrometer is sufficient to separate events with missing pions, as shown in this comparison of the reconstructed mass distributions of $B^0 \to \pi^+\pi^-$ and $B^0 \to \pi^+\pi^-\pi^0$.

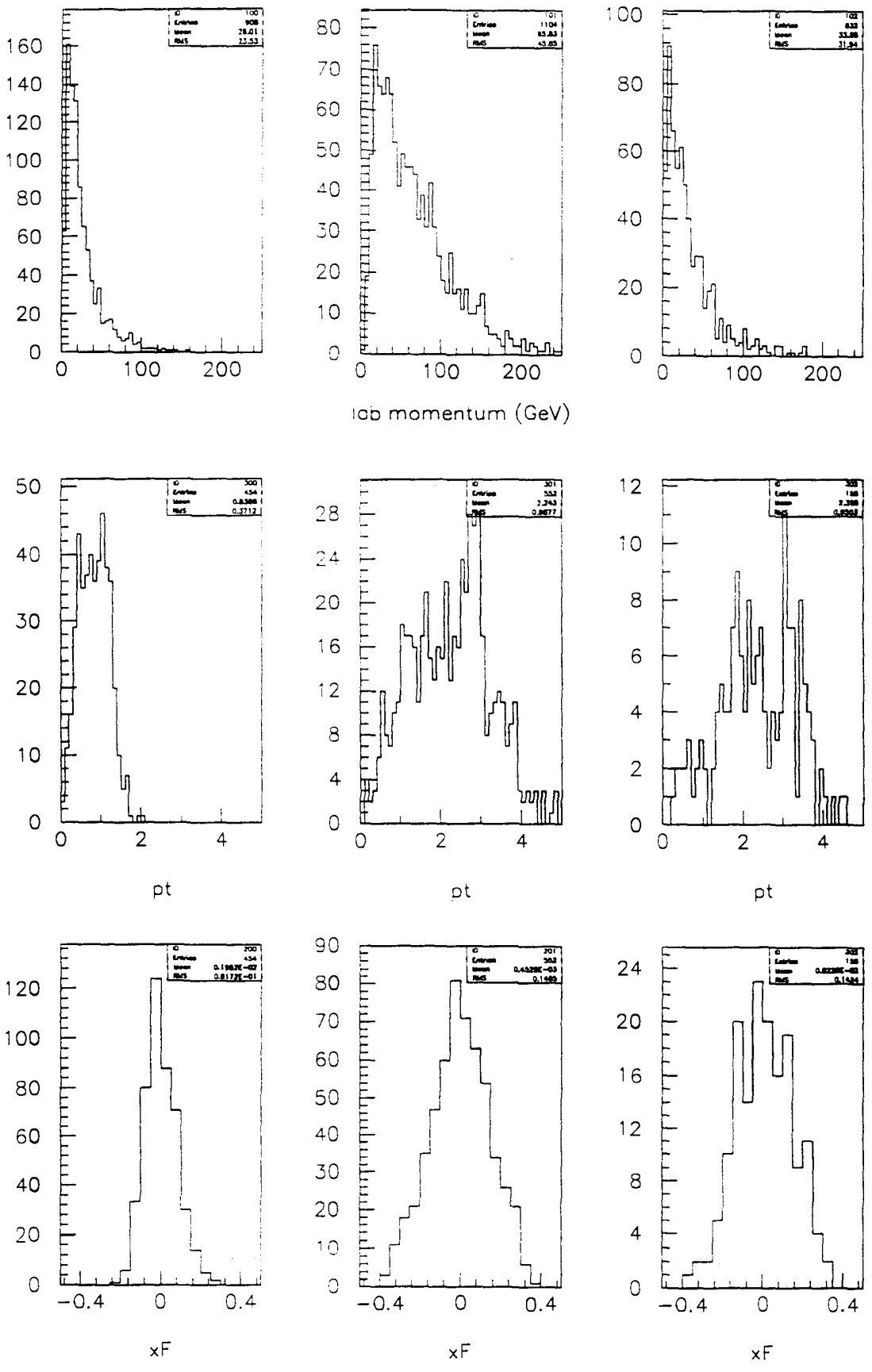

Figure I.1 - The single-particle momentum spectra, x_F, and p_t distributions of accepted charm and beauty decays: left $D^0 \to K^-\pi^+$, middle $B^0 \to \pi^+\pi^-$, right $B^0 \to J/\psi K_s$.

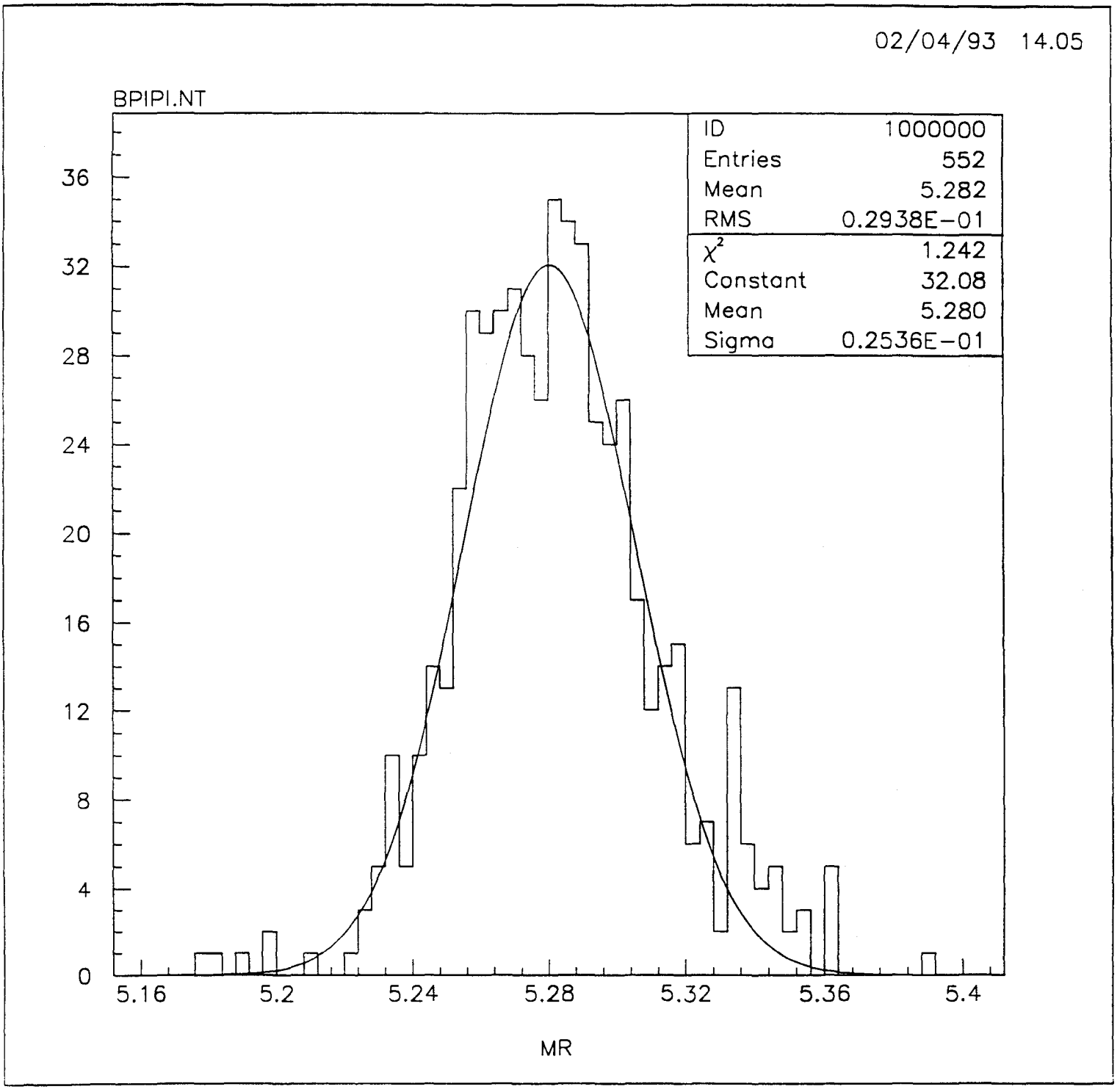

Figure I.2 - The reconstructed mass distribution for $B^0 \rightarrow \pi^+\pi^-$ decays.

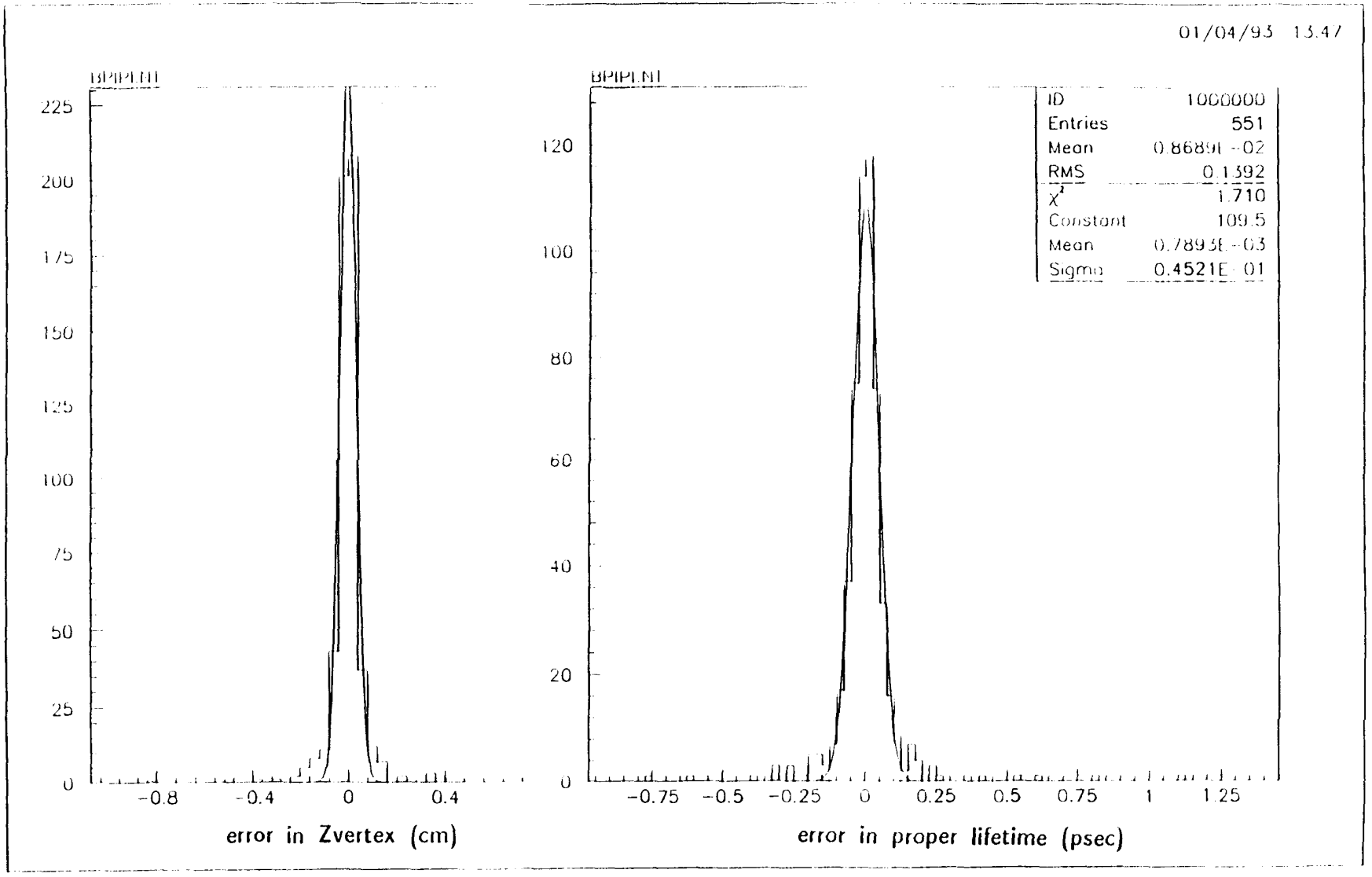

Figure I.3 - The resolution in decay distance ($z_{\text{reconstructed}} - z_{\text{thrown}}$) and in proper time ($\tau_{\text{reconstructed}}$) of P865.

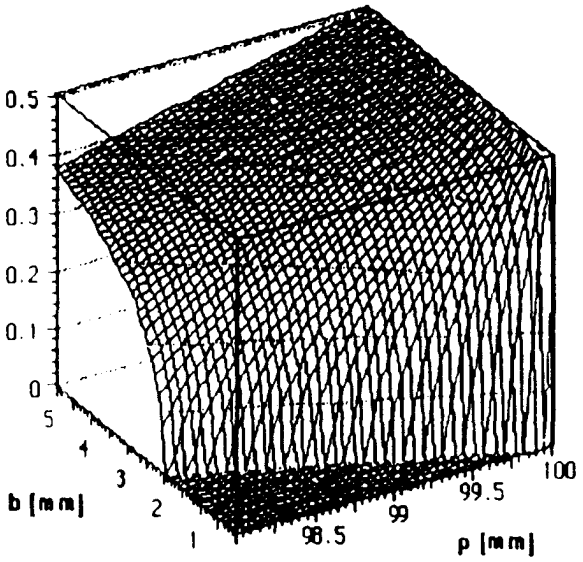

Refractive index n = √2

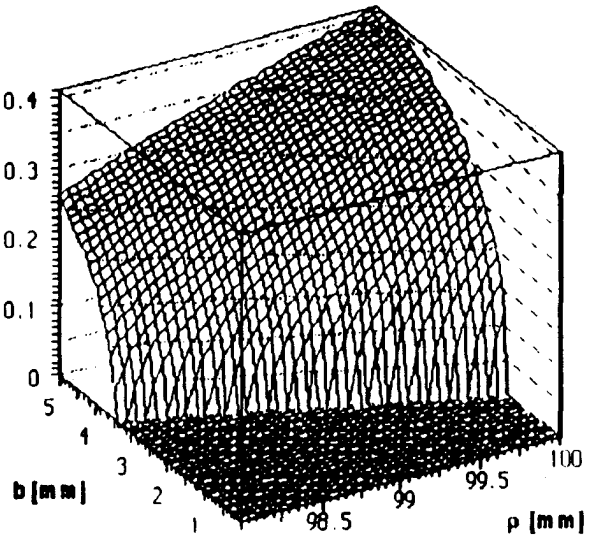

Refractive index n = √2 - 0.01

Probability for a Cherenkov photon to be trapped, as a function of the depth ρ where it was produced inside the crystal and of the impact parameter b of the incident charged particle. Two values of the refractive index are considered.

Figure III.1

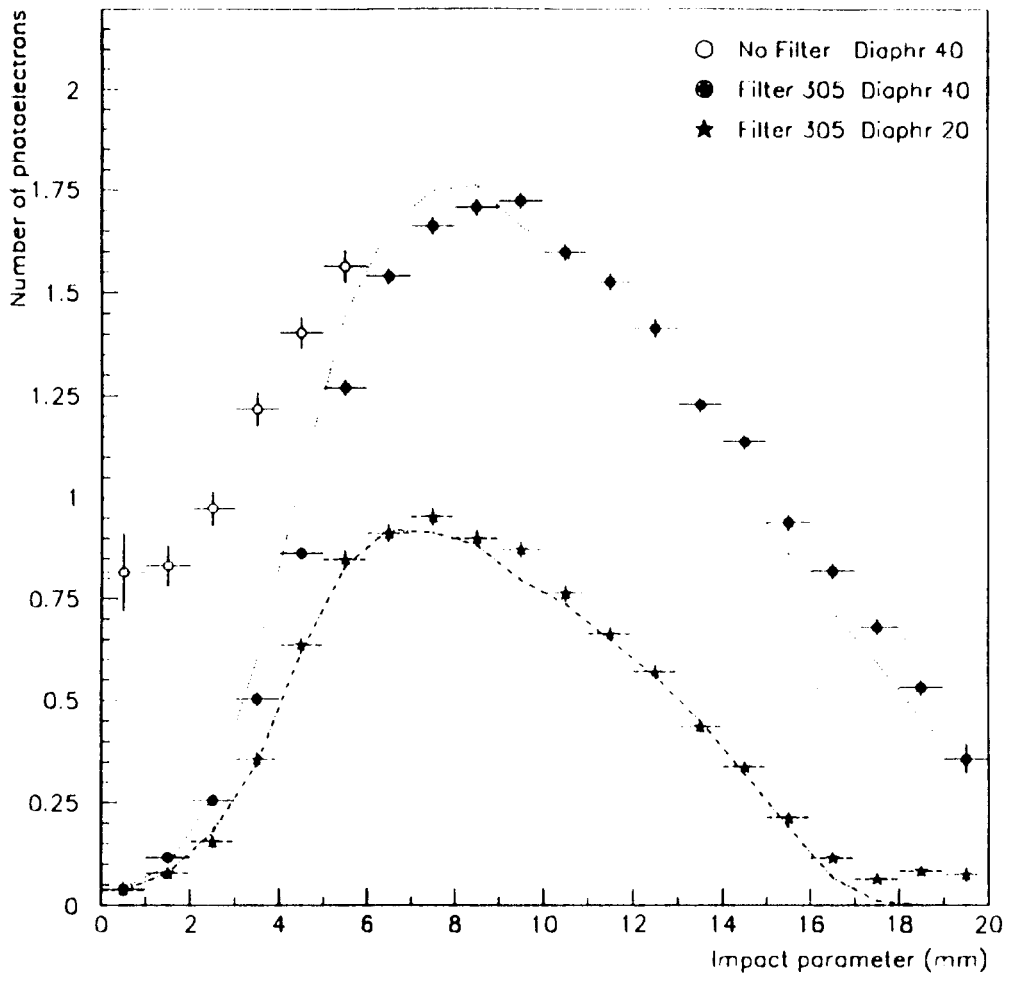

Amplitude of the signal as a function of the impact parameter with and without filter and with two different diaphragms.

Figure III.2

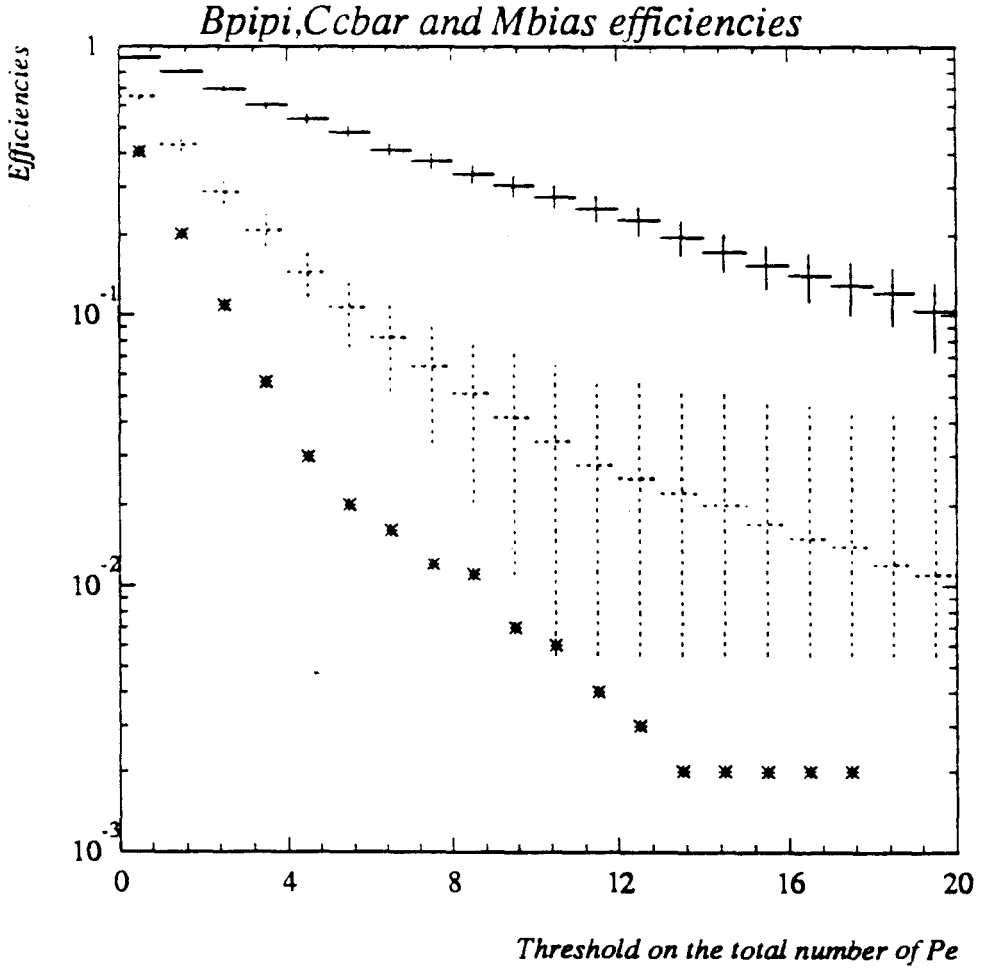

Figure III.3 - The efficiencies for minimum-bias, charm,and beauty events (with one B decaying in the $\pi^+\pi^-$ channel and the other decaying at random), plotted as a function of the threshold applied to the total number of photoelectrons detected.